UNC-10/SYD-2 complex is sufficient to link kinesin-3 UNC-104 to RAB-3 containing synaptic vesicles in the absence of the motor's PH domain

Prerana Bhan, Odvogmed Bayansan, Chien-Yu Chang and Oliver Ingvar Wagner*

National Tsing Hua University, Institute of Molecular and Cellular Biology, Department of Life Science, Hsinchu, 30013, Taiwan (R.O.C.)

Running title: The effect of RAB-3-UNC-10-SYD-2 complex on UNC-104.

***Corresponding author**:

Dr. Oliver I. Wagner

Professor

National Tsing Hua University

Institute of Molecular and Cellular Biology & Department of Life Science

101, Sec. 2, Kuang-Fu Road, Hsinchu 30013, Taiwan (R. O. C.)

Email: owagner@life.nthu.edu.tw

Phone: +886-3-574-2487, Fax: +886-3-571-5934

Keywords: SYD-2, UNC-10, RAB-3, kinesin-3, SNB-1, UNC-104.

Conflicts of interest: The authors declare no conflict of interest.

ABSTRACT

KIF1A (UNC-104 in *C. elegans*) is the major fast axonal transporter of STVs (synaptic vesicle protein transport vesicles) containing synaptic precursors such as RAB-3 or synaptobrevin-1 (SNB-1). Heritable mutations in neuronal motor proteins (and their adaptors) lead to numerous neurodegenerative diseases. The C-terminal PH (pleckstrin homolog) domain of UNC-104 directly binds to phosphatidylinositol 4,5-bisphosphate that form the lipid bilayers of STVs. Based on literature evidences, we hypothesize that RAB-3-bound STVs may employ a dual linker UNC-10/SYD-2 to connect to UNC-104. This RAB-3/UNC-10/SYD-2 linker may act as an additional reinforcement for the (supposed) weak motor-lipid interaction. Results from RT-PCR and Western blot experiments favor a genetic relation between SYD-2, UNC-10 and RAB-3, as well as co-immunoprecipitation assays revealed changes in binding affinities between SYD-2 and UNC-104 depending on the presence or absence of UNC-10 or RAB-3. Such changes in binding properties between SYD-2 and UNC-104 (depending on *unc-10* and *rab-3*) can be also seen in colocalization and BiFC (bimolecular fluorescence complementation) assays. In sublateral neuronal bundles, as well as in single ALM mechanosensory neurons, UNC-104 expression appears to be more diffused and is restricted to short travel distances (with visibly reduced speeds) in *unc-10* and *rab-3* mutants. Similar results were revealed when observing RAB-3-containing vesicles but not synaptobrevin-1 (SNB-1)-containing vesicles. Moreover, deletion of UNC-104's PH domain did not affect UNC-104/RAB-3 colocalization while it did affect UNC-104/SNB-1 colocalization. These findings solidly support the model a dual UNC-10/SYD-2 linker acting as a sufficient buttress to connect the motor to RAB-3-containing vesicles.

INTRODUCTION

Understanding the molecular basis of axonal transport is critical to develop novel drugs to prevent or cure various neurological diseases such as Charcot–Marie–Tooth disease (CMT), Amyotrophic lateral sclerosis (ALS) or Alzheimer's disease (Breuss and Keays, 2014; Brooks, 1991; Franker and Hoogenraad, 2013). The neuronal cytoskeleton is composed of microtubules (MTs), actin filaments as well as neurofilaments (NFs) all functioning to maintain neuronal polarity, morphology and integrity of axons (Barnes and Polleux, 2009; Kapitein and Hoogenraad, 2011; Luo, 2002). Axonal transport supplies axons and nerve terminals with proteins, lipids and mitochondria and prevents the build-up of misfolded proteins and toxic aggregates (Perlson et al., 2010). Kinesins move from the minus-ends to plus-ends of uniform oriented MTs in axons (anterograde transport) thereby transporting STVs (synaptic vesicle protein transport vesicles) from neuronal cell bodies (somas) to axonal termini while retrograde transport is solely accomplished by dynein (Maday et al., 2014). KIF1A is a neuron-specific molecular motor belonging to the kinesin-3 family and is termed as UNC-104 in *C. elegans.* UNC-104 is the major fast axonal transporter of synaptic vesicle precursors such as RAB-3, synaptotagmin, synaptobrevin and synaptophysin (Hall and Hedgecock, 1991; Maeder et al., 2014). KIF1A-deficient mice die at the embryonic stage due to degeneration of sensory neurons based on vesicle retention phenotypes in somas (Yonekawa et al., 1998). A similar vesicle retention phenotype can be observed in *C. elegans unc-104* mutants and these axonal transport defects lead to paralyzed worms, however, being able to feed and survive (Hall and Hedgecock, 1991). *Unc-104* mutants also bear structural defective active zones providing evidence for a function role of UNC-104 in site-specific synapse maturation (Zhang et al., 2016). Critically, mutations in KIF1A/UNC-104 - leading to axonal transport defects - have been associated to various neurological disorders such

as CMT and ALS (Brady and Morfini, 2017; Millecamps and Julien, 2013). In *C. elegans*, UNC-104 associates with Tau/PTL-1 and mutations in *ptl-1* affect the transport behavior of the motor (Tien et al., 2011). KIF1A motors are inactive, or undergo slow biased processivity, when being in the monomeric state; however, quickly dimerize (via their coiled coil domains) upon cargo binding resulting in immediate fast and directed processivity (Rashid et al., 2005). The PH (pleckstrin homology) domain of UNC-104 tightly binds to phosphatidylinositol 4,5-bisphosphate (PtdIns(4,5)P_2) in membranes of STVs, and when accumulating in lipid rafts, motors tend to efficiently dimerize for fast processivity (Klopfenstein and Vale, 2004).

The active zone is the site of synaptic vesicle docking and fusion involving a variety of proteins such as Munc-13/UNC-13, Rab-3/RAB-3, Rim-1/UNC-10, Liprin-α/SYD-2, CASK/LIN-2 or Clarinet/CLA-1. Direct and functional interactions between active zone components and UNC-104 have been reported such as UNC-104/SYD-2 (Wagner et al., 2009), UNC-104/RAB-3 (Nonet et al., 1997), UNC-104/CLA-1 (Xuan et al., 2017) and UNC-104/LIN-2 (Wu et al., 2016). *C. elegans.* SYD-2 is a multi-domain scaffolding protein that comprises of eight N-terminal coiled coils and three C-terminal sterile alpha motifs (SAM domains) that are able to interact with each other (intramolecular folding) to inactive the proteins physiological function (Chia et al., 2013). Further, multiple SYD-2 proteins are able to form a scaffold (Spangler and Hoogenraad, 2007). In *syd-2 loss of function* mutants active zones appear diffuse and less regular along axons causing impairment of synaptic vesicle docking and synaptic transmission (Kittelmann et al., 2013; Stigloher et al., 2011; Zhen and Jin, 1999). The N-terminal domain of SYD-2 directly associates with other synaptic proteins such as CAST/ELKS, GIT1 and RIM/UNC-10 (Ackermann et al., 2015; Dai et al., 2006; Ko et al., 2003; Shin et al., 2003; Spangler et al., 2013) while the C-terminal SAM domains interact with the FHA domain of UNC-104 to activate the motor (Wagner et al.,

2009). Both SYD-2 and UNC-104 inherit dual roles in maintaining synaptic vesicle cluster stability and transport (Edwards et al., 2015). SYD-2/RAB-3 interactions are reported to maintain the synaptic vesicle pool at presynaptic dense projections (Wu et al., 2013). RIMs are a family of multi-domain scaffolding proteins that were initially identified as putative Rab3 effectors that regulate synaptic vesicle fusion (Wang et al., 1997). The RIM homolog identified in *C. elegans* is UNC-10 (Koushika et al., 2001) composed of an N-terminal zinc finger motif, a central PDZ domain, two C-terminal C2 domains (C2A and C2B) and a short proline-rich SH3 motif (Wang et al., 2000). RIM/UNC-10 interacts with multiple synaptic proteins and one example is that its N-terminal zinc finger domain interacts with GTP-bound Rab3 (Wang et al., 1997) while its C-terminal C_2B domain associates with the N-terminus of Liprin-α/SYD-2 (Schoch et al., 2002). Liprin-α regulates the presynaptic organization by anchoring RIM1 and CASK to facilitate synaptic vesicle release (Spangler et al., 2013) and it has been shown that UNC-10 and SYD-2 act in the same pathway to regulate synaptic vesicle turnover (Stigloher et al., 2011). Based on the aforementioned direct and functional interaction between UNC-10 and SYD-2 one may speculate a role of UNC-10 in regulating UNC-104. We hypothesize that the interaction between UNC-104 and a RAB-3-bound synaptic vesicles may be strengthen via a proposed tripartite linker RAB-3/UNC-10/SYD-2. Critically, all three active zone proteins SYD-2, UNC-10 and RAB-3 colocalize with each other and are also co-transported in *C. elegans* DA9 motor neurons (Wu et al., 2013).

Rab3/RAB-3 is a member of the RAB family of small GTPases that recruits synaptic vesicles for vesicle docking and fusion at active zones (Geppert et al., 1994). It integrates into the synaptic vesicle membrane via its C-terminal sequence Cys-X-Cys that is highly conserved in invertebrates (Johnston et al., 1991). Rab3A binds to synaptic vesicles in its GTP-bound state and

dissociation occurs after GTP-hydrolysis (Fischer von Mollard et al., 1994). The guanine nucleotide exchange factor (GEF) AEX-3 (DENN/MADD) plays an important role in regulating RAB-3, concomitantly affecting proper localization of presynaptic proteins and neurotransmitter release (Mahoney et al., 2006). Rab3A is transported to the active zone by the fast anterograde axonal transport system in axons (Li et al., 1995) and KIF1A associates to Rab3-carrying vesicles via DENN/MADD (Niwa et al., 2008). Rab3A null mutant mice (Geppert et al., 1994) and worms (Nonet et al., 1997) display mild behavioral abnormalities, whereas worms specifically reveal resistance to aldicarb, perturbed synaptic transmission and fewer synaptic vesicles near the active zone (indicating impaired synaptic vesicle transport) (Nonet et al., 1997). Active zone proteins SYD-2, UNC-10 and RAB-3 colocalize with each other and are also co-transported in *C. elegans* DA9 motor neurons (Wu et al., 2013). In another study, it has also been shown that SYD-2 colocalizes with UNC-104 (Wagner et al., 2009). Besides RAB-3, the synaptic precursor SNB-1 (Synaptobrevin-1) has been well characterized in *C. elegans* (Nonet et al., 1993). Worms lacking SNB-1 are embryonically lethal due to disturbed synaptic transmission and in *unc-104* mutants SNB-1 retention in somas is observed (Nonet et al., 1998).

Due to the characterized weak and non-specific binding between PH domains and lipid bilayers (Lemmon and Ferguson, 2001), and based on the aforementioned knowledge from the literature, we propose that RAB-3 containing vesicles would reveal additional support to UNC-104 via UNC-10 and SYD-2 (RAB-3 -> UNC-10 -> SYD-2 -> UNC-104).

RESULTS

Genetic relation between *syd-2*, *unc-10* and *rab-3* in worms

Even though the relation between Liprin-α/SYD-2 and RIM/UNC-10 as well as Rab3/RAB-3 has been well described in the literature (see Introduction), we intended to confirm the genetic relation between SYD-2 and UNC-10 as well as RAB-3 in worms. As a result, *syd-2* expression levels increase in *unc-10(md1117)* and *unc-10(e102)* allelic mutant backgrounds by 1.3~1.5 fold (Figure 1A; *syd-2* expression normalized to endogenous *cdc-42* as internal control). The strain NM1657 *(md1117)* carries a large 8601 bp deletion in the *unc-10* gene that includes the entire coding region along with regions of the 5' and 3' UTRs and it is likely a knockout (Suppl. Figure S1A). The phenotype is coiler and uncoordinated (Koushika et al., 2001). The strain CB102 *(e102)* is a C to T substitution in intron 15 of the *unc-10* gene resulting in splicing defects and produces a truncated protein that excludes the C-terminal domain (Koushika et al., 2001) (Suppl. Figure S1A). Contrary to the increased expression of SYD-2 in *unc-10* mutant worms, its expression is decreased by 50% in *rab-3(js49)* mutants (Figure 1B; *syd-2* expression normalized to *cdc-42*). The strain NM791 *(js49)* is a G to A transition at position 2 of the tryptophan 76 codon in the *rab-3* gene leading to a nonsense mutation causing a premature stop (Nonet et al., 1997) (Suppl. Figure S1A). Note that two other strains NM210 and 211 exist carrying *rab-3* alone, however, these strains are poorly characterized as well as the worm phenotypes are less drastic as opposed to the *js49* strain. Also note that the changes in SYD-2 expression as shown in Figure 1A+B go well along with changes in protein expression (Figure 1C+D; for gels please refer to "Lysate" in Figure 1E and G, respectively).

Effects of *unc-10* and *rab-3* mutations on the UNC-104/SYD-2 complex

The interaction between SYD-2 and UNC-104 has been well described (see Introduction) and as a first approach to understand whether UNC-10 and RAB-3 plays a role in this functional interaction, we performed co-immunoprecipitation experiments. Precipitating UNC-104::GFP (using an anti-GFP antibody) from whole worm lysates, we found that bound SYD-2 was reduced in both *md1117* and *e102* mutant backgrounds (Figure 1E+F) (for antibody details, refer to Methods & Materials). Similarly, precipitating UNC-104::mRFP from whole worm lysates (using an anti-RFP antibody), SYD-2 expression was significantly reduced in *js49* mutants (Figure 1G+H). These data point to a functional relation between the UNC-104/SYD-2 complex and UNC-10 as well as RAB-3. To understand whether UNC-104/SYD-2 interactions also visibly change in neurons of worms, we performed co-colocalization as well as bimolecular fluorescence complementation (BiFC) assays. In BiFC assays, the YFP protein Venus is split into two halves (N-terminal Venus, VN, and C-terminal Venus, VC) and test proteins are labeled with each half. Complementation of Venus, thus, yellow fluorescent signals, occurs only if the two test proteins are at least 7-10 nm close to each other, therefore likely forming functional complexes (Hsu et al., 2011; Hu and Kerppola, 2003). Our data reveals that colocalization between UNC-104 and SYD-2 in nerve rings significantly decreases in *md1117* and *js49* mutants as well as in *md1117* and *js49* double mutants (Figure 2A+B). More importantly, physical interactions between UNC-104/SYD-2 complexes (as revealed by BiFC experiments) are disrupted in *md1117* and *js49* mutants (Figure 2C+D). These data are consistent with our *in vitro* observations from Figure 1 and support our hypothesis that UNC-104/SYD-2 complexes are dependent on the presence of UNC-10 and RAB-3.

Role of *syd-2*, *unc-10*, *rab-3* mutations (and their combinations) on UNC-104 particle distribution in neurons

To analyze the physiological consequences of our observations, we observed changes in UNC-104 motor distributions in neurons in single (*syd-2*, *unc-10* and *rab-3*) and double mutants (*syd-2*/*unc-10*, *syd-2*/*rab-3*, *rab-3*/*unc-10*). Previously, we reported that UNC-104 clusters along axons in an arrangement that does not match known *en passant* synapse patterns as well as demonstrated that those clusters were dynamic structures rather than inactive motor aggregates (Wagner et al., 2009). In this study, we analyzed UNC-104 cluster formation in the sublateral system (subdorsal and subventral neuron bundles comprised of various motor-, sensory- and inter-neurons) and a single (long) mechanosensory neuron (ALM) (Suppl. Figure S1B). Though the focus lied in analyzing the single ALM neuron, it is evident that in both types of neurons (bundles) UNC-104 aggregates became significantly smaller in *unc-10* and *syd-2* mutants (as well as in *rab-3* mutants when inspecting the ALM neuron) (Figure 3A-C and E; Suppl. Table S1). Critically, these reduction in UNC-104 cluster sizes could be rescued by introducing the wild type gene into the respective mutant backgrounds (Figure 3E). Though double mutants did not induce significantly smaller cluster sizes (as opposed to their single mutant counterparts) they, on the other hand, also neither rescued nor enhance the effects as observed for the single mutants (except for *syd-2*;*unc-10* cluster sizes are not significantly different from wild type sizes) (Figure 3C+E). We also analyzed the travel distances of UNC-104 particles from the proximal axon hillock to distal areas of the ALM neuron (Suppl. Figure S1B). Data summarized in Figure 3D show that motor travel distances are significantly reduced in *syd-2* and *unc-10* mutants (and could be rescued by introducing the respective wild type gene), however not in *rab-3* mutants. In *rab-3*;*unc-10* as well as *syd-2;unc-10* double mutants travel distances are significantly reduced and, interestingly, in *rab-3*;*syd-2*

mutants travel distances even increase (Figure 3C+D) pointing to an unknown compensating pathway. Nevertheless, nearly all double mutants significantly vary the effects as seen in single mutants points to the strong interdependence of these genes on regulating UNC-104 displacements. Especially that *rab-3* significantly decreased the *unc-10* effect is in accordance with our model of *rab-3* being tightly linked to *unc-10*. Since reduction in UNC-104 travel distances is likely related to diminished motor speeds we therefore analyzed UNC-104 motility parameters.

Role of *syd-2*, *unc-10*, *rab-3* mutations (and their combinations) on UNC-104 motility

To track UNC-104 in the long (up to 500 μm) ALM neurons, we tagged its C-terminal end with mRFP (spaced by a flexible linker) that is reported to be less prone to self-aggregation as opposed to GFP (Campbell et al., 2002). Kymograph analysis (Suppl. Figure S1C) from recorded videos enables us to calculate various parameters such as motor velocity, total run-length, moving persistence and pausing (see Material & Methods). As expected, all single genes *syd-2*, *unc-10* and *rab-3* significantly reduce UNC-104 moving speeds (Figure 4A, Suppl. Figure S2A, Suppl. Table S3). Though run lengths were unchanged in these genetic background, we were able to boost run length when overexpressing SYD-2 (Figure 4B, Suppl. Figure S2B, Suppl. Table S3). Furthermore, both velocities as well as motor run lengths were significantly reduced in *rab-3* double mutants *rab-3*;*unc-10* and *rab-3*;*syd-2* once more pointing to string synergistic effects between these genes. Notably, in the *rab-3*;*unc-10* double mutant with especially low velocities and reduced run lengths also the number of pauses (per 100 μm) increases (Figure 4D, Suppl. Table S4) consistent with observations for very small travel distances for this double mutant as shown in Figure 3C+D. The parameter anterograde persistency reflects the time an UNC-104 particle moves without pausing. These parameters are inversely proportional to motor speeds (Figure 4C, Suppl. Table S4) likely due to the assumption that faster motors are easier to lose track as opposed to slower ones. This

increased time spending on microtubules (likely due to slower speeds) goes well along with measured less number of pauses per 100 μm (Figure 4D). Note that we were able to successfully rescue all seen effects on the single mutants (Figure 4A-D). In conclusion, single and double mutant analysis points to strong synergistic effects between RAB-3, UNC-10 and SYD-2 to regulate UNC-104 motility.

UNC-10/SYD-2 complex is required for RAB-3 but not for SNB-1 based transport

Based on our hypothesis as shown in Figure 7C only RAB-3-containing synaptic vesicles may profit from a stabilizing linker (to tightly bind UNC-104) while other precursors, such as SNB-1, may not gain such advantage. Based on this conception we analyzed motility as well as travel distances of both mCherry::RAB-3 as well as SNB-1::mRFP tagged synaptic vesicles in different mutant backgrounds (Figure 5). Because the universal UNC-104-activating effect of SYD-2 on synaptic vesicle transport (such as on RAB-3 as well as SNB-1-bound vesicles) has been well reported (Wagner et al., 2009; Wu et al., 2016), it is not surprising to see reduced speeds of both SNB-1- and RAB-3-tagged vesicles (Figure 5A+B, Suppl. Table S5). However, only the speeds as well as run-lengths of RAB-3-bound vesicles are affected by the *unc-10*(*md1117*) allele. Similarly, this mutation only affects visible travel distances in ALM neurons (Figure 5E-H, Suppl. Table S6). Interestingly, RAB-3-bound vesicles cover generally larger travel distances as compared to SNB-1-bound vesicles (Figure 5, wild type data). As a control we knocked down *rab-3* in SNB-1::mRFP expressing worms and *snb-1* in mCherry::RAB-3 expressing worms not revealing any significant effects on vesicles speeds (Figure 5A+B). Critically, *syd-2* RNAi in *unc-10* mutant backgrounds does lead to impairments in SNB-1 transport once more emphasizing the importance of SYD-2 on UNC-104-based vesicle transport. These data go well along with our proposed model as shown in Figure 7C.

Dual linker UNC-10/SYD-2 is sufficient to associate UNC-104 to RAB-3 bound vesicles in the absence of the motor's PH domain

Based on our proposed model as shown in Figure 7 if eliminating UNC-104's PH domain the motor may still be able to effectively transport RAB-3 vesicles. To understand whether this assumption is correct or not, we designed worms double expressing a green fluorescent motor with a deleted PH domain as well as either red fluorescent RAB-3-tags or SNB-1-tags. Our colocalization analysis (using ICQ quantification, see Materials and Methods) revealed that UNC-104 and RAB-3 vesicles do still colocalize in wild type animals even in the absence of the PH domain (Figure 6A+B and D, Suppl. Figure S3A+B line scans) whereas the motor does not colocalize with SNB-1 vesicles in the absence of the PH domain (Figure 6E and F, Suppl. Figure S4A+B line scans). This effect (SNB-1 does not colocalize with UNC-104ΔPH, but RAB-3 does colocalize with UNC-104ΔPH) is also obvious in dorsal (Figure 6G) and ventral (Figure 6H) nerve cords (note that cell bodies of motor neurons are present in ventral nerve cords but not in dorsal nerve cords). More importantly, in *syd-2* as well as in *unc-10* mutants colocalization between UNC-104 and RAB-3 vesicles is ultimately disrupted (Figure 6C+D, Suppl. Figure S3C+D). Notably, the *unc-10* mutation does not have any effect on UNC-104 and SNB-1 colocalization (Figure 6E+F, Suppl. Figure S4C).

DISCUSSION

The multifaceted functions and interaction sites of active zone proteins have been extensively studied. A key player in the pre-synaptic active zone complex is apparently liprin-α/SYD-2 that encompasses binding sites for KIF1A/UNC-104, RIM/UNC-10, CAST, GIT, as well as LAR/PTP-3 receptor. RIM/UNC-10 itself binds to RAB3/RAB-3, liprin-α/SYD-2, Munc-13 and CAST binding sites (Zhen and Jin, 2004). Based on this knowledge, we proposed a model in which Rab-3 containing vesicles (but not SNB-1 containing vesicles) would benefit from an additional linkage that would support their binding to kinesin-3 UNC-104 (Figure 7). How motors bind and recognize their cargo is vividly discussed in the literature (Brady and Morfini, 2017; Franker and Hoogenraad, 2013; Maday et al., 2014), and the proposed tripartite (SYD-2/UNC-10/RAB-3) linkage complex may act as a novel receptor for UNC-104 to selectively transport RAB-3 containing vesicles. Because the well-described linkage of UNC-104 to vesicular structures via the motor's PH domain (Klopfenstein and Vale, 2004) is generally weak and rather non-specific (Lemmon and Ferguson, 2001) our proposed linker would provide the motor additional support and increase binding specificity. Our model is supported by findings that SYD-2/UNC-10, UNC-10/RAB-3 and SYD-2/RAB-3 all colocalize and are co-transported (Wu et al., 2013). Furthermore, liprin-α/SYD-2 also affects the transport of dense-core vesicles (Goodwin and Juo, 2013) and RIM1α/UNC-10 (known to be a dense-core vesicle protein) as well as RAB-3 are mislocalized in *liprin-α/syd-2* mutants.

Our results reveal a tight genetic linkage between UNC-10 and SYD-2 (Figure 1A-D) as well as on their physical binding to UNC-104 (Figure 1E-H). The physiological consequences of this tight linkage between UNC-10 and SYD-2 on UNC-104 neuronal distribution (Figure 2-3), UNC-104 motility (Figure 4) and UNC-104 mediated RAB-3 vesicle transport (Figure 5-6) are evident. Indeed, it has been reported that UNC-10 acts as a stabilizer of SYD-2 and that UNC-10

binding to the C-terminus of SYD-2 also facilitates SYD-2's oligomerization (Chia et al., 2013; Taru and Jin, 2011). The importance of oligomerized SYD-2 lies in its proposed function as a motor scaffolding protein that may bind to more than one UNC-104 (via SYD-2's SAM domains) at the same time (Chia et al., 2013; Wagner et al., 2009). Similarly, the tight relation between UNC-10/SYD-2 to RAB-3 is obvious from our experiments, e.g., precipitating UNC-104::mRFP from whole worm lysates bound SYD-2 is obviously reduced in *rab-3(js49)* mutant animals (Figure 1G+H). The absence of rab-3 negatively affects both UNC-104 neuronal distribution (Figure 3E) as well as motor speeds (Figure 4A) and these effects are significantly enhanced in the presence of *unc-10* mutations (Figures 3D+E and 4A). UNC-104 requires *arl-8*, a small GTPase to unlock its autoinhibitory state (Niwa et al., 2016). Because ARL-8 is usually tightly associated with the cargo vesicle, it is possible that in the absence of *rab-3* not only motor-cargo association is compromised, but also might promote inactivation of UNC-104. Enhanced intramolecular folding of UNC-104 would then in turn mask SYD-2 binding sites consistent with seen effects in co-immunoprecipitation assays (Figure 1G+H). Critically, a study that dissected the direct interactions between RAB-3 and UNC-10 in *C. elegans* suggests epistatic regulation of these proteins (Gracheva et al., 2008). It has been also shown that in *syd-2* mutants UNC-10 and RAB-3 mislocalize to dendrites in DA neurons (Goodwin and Juo, 2013). Furthermore, loss of *syd-2*, *unc-10* and *rab-3* cause depletion of synaptic vesicles at the dense projection (Stigloher et al., 2011). To interpret measured *rab-3* effects, we also need to consider the enhancing or compensating effects by other Rabs that may exhibit partial overlapping functions to RAB-3, such as RAB-27, which is a close homolog of RAB-3 regulated by AEX-3/DENN/MADD (Mahoney et al., 2006; Niwa et al., 2008). On the other hand, it has been shown that various synaptic vesicle precursor are transported in a RAB-independent fashion (Niwa et al., 2008) consistent with our

observations on RAB-3 independent transport of SNB-1, and, more critically, we have also shown that SNB-1 transport is independent of UNC-10 (Figure 5+6). Moreover, the overall slower movement of SNB-1, as opposed to RAB-3 (Figure 5, Suppl. Table S5), may lead to the assumption that more UNC-104 motors may bind to a single RAB-3 vesicle, thus speeding up transport speeds, consistent with the multiple motor model (Vershinin et al., 2007).

The strong negative effects of single *unc-10* mutations on UNC-104 neuronal distributions (Figure 3) as well as motor motility (Figure 4) may lead to the notion that UNC-10 stabilizes the binding of SYD-2 to UNC-104 (Figure 7). Loss of UNC-10 would subsequently lead to loss of SYD-2 binding, therefore leading to motor inactivation as well as reduced axonal clustering (Wagner et al., 2009; Wu et al., 2016). This assumption is in accordance with observations that unc-10 RNAi even reduces seen SYD-2 overexpression effects (boosting motor speeds, Figure 4A). The idea of a dual UNC-10/SYD-2 linker (supporting the binding of UNC-104 to RAB-3 bound vesicles) is only valid if deleting the motor's PH (Pleckstrin homology) domain would not affect motor RAB-3 vesicle interactions. Indeed, we have shown that deleting the motor's PH domain does not affect the motor-RAB-3 vesicle interaction whereas it does affect motor-SNB-1 vesicle interaction (Figure 6). Binding between PH domains and membranous phosphoinositides is rather weak and non-specific (Lemmon and Ferguson, 2001) and the overall strength of lipid-protein interactions depend on the various membranous lipid constituents (Richens et al., 2015). Also, varying vesicular membrane charges may modulate protein-lipid interactions (Richens et al., 2015). Therefore, although protein-lipid interaction seems to be imperative for UNC-104-vesicle interactions (Klopfenstein et al., 2002), both specificity and binding-strength of such interactions are generally low. The dual linker SYD-2/UNC-10 may be therefore critical to strengthen the motor-vesicle interaction. Moreover, because UNC-104 undergoes dimerization upon membrane-

cargo binding (Klopfenstein et al., 2002; Tomishige et al., 2002), such an additional linker may prolong the motor's activated state.

MATERIALS & METHODS

C. elegans strains and plasmids

Worms were maintained at 20°C on NGM agar plates seeded with OP50 *E. coli* according to standard methods (Brenner, 1974). Transgenic animals *Punc-104::unc-104::gfp(e1265), Punc-104::unc-104::mrfp(e1265) and Punc-104::unc-104::mrfp(ok217)* were described previously (Tien et al., 2011; Wagner et al., 2009). Strain *Punc-104::unc-104ΔPH::gfp(e1265)* is a kind gift from Dr. Dieter Klopfenstein (Georg-August-University, Göttingen, Germany) (see also (Klopfenstein and Vale, 2004)). The existing constructs *Punc-104::unc-104::gfp* and *Punc-104::unc-104::mRFP* were microinjected at a concentration of 100 ng/µl into *unc-10(md1117)* and *rab-3(js49)* mutant worms to generate transgenic lines OIW 77 *unc-10(md1117);nthEx77[Punc-104*::*unc-104::mrfp],* OIW 78 *unc-10 (md1117);nthEx78[Punc-104*::*unc-104::gfp] and* OIW 79 *rab-3(js49);nthEx79[Punc-104*::*unc-104::mrfp]* , respectively. Mutant strains were received from the Caenorhabditis Genetics Center (Minnesota, USA). For colocalization studies, existing plasmid *Punc-104::gfp::syd-2* was co-injected along with *Punc-104::unc-104::mrfp* (each at a concentration of 75 ng/µl) into N2 wild type animals, *unc-10(md1117)* and *rab-3(js49)* mutants animals to obtain strains OIW 80 N2;*nthEx80[Punc-104::gfp::syd-2;Punc-104::unc-104::mrfp*], OIW 81 *unc-10 (md1117)*;*nthEx81[Punc-104::gfp::syd-2;Punc-104::unc-104::mrfp]* and OIW 82 *rab-3(js49)*;*nthEx82[Punc-104::gfp::syd-2;Punc-104::unc-104::mrfp]*. Likewise, *Punc-104::gfp::syd-2* (75 ng/µl) was microinjected into *unc-10(md1117);rab-3(js49)[Punc-104::unc-104::mrfp]* to obtain OIW 83 *unc-10(md1117),rab-3(js49)*; *nthEx83[Punc-104::gfp::syd-2;Punc-104::unc-104::mrfp]*. Note that for optimal operation of the Punc104 promoter rather high

injection dosages are needed (Tien et al., 2011; Wagner et al., 2009). For BiFC (bimolecular fluorescence complementation) studies following strains were generated using existing plasmids *Punc-104::unc-104::VC155* and *Punc-104::VN173::syd-2* (Hsu et al., 2011): OIW 84 N2;*nthEx84[Punc-104::unc-104::VC155;Punc-104::VN173::syd-2]*, OIW 85 *unc-10(md1117)*;*nthEx85[Punc-104::unc-104::VC155;Punc-104::VN173::syd-2]* and OIW 86 *rab-3(js49); nthEx86[Punc-104::unc-104::VC155;Punc-104::VN173::syd-2]*, respectively. For *rab-3* rescue strains we generated *Punc-104::rab-3::yfp* and injected it at 75 ng/µl into *rab-3(js49);nthEx[Punc-104*::*unc-104::mrfp]* mutant strain to create OIW 87 *rab-3(js49);nthEx87[Punc-104*::*unc-104::mrfp; Punc-104::rab-3::yfp]*. Likewise, *unc-10* rescue strains were generated by cloning *Punc-104::unc-10::gfp* and injecting it at 75 ng/µl into *unc-10(md1117);nthEx[Punc-104*::*unc-104::mrfp]* mutant strain to create OIW 88 *unc-10(md1117);nthEx88[Punc-104*::*unc-104::mrfp; Punc-104::unc-10::gfp]*. Similarity, *syd-2* rescue strains were obtained by co-injecting existing plasmid *Punc-104::gfp::syd-2* along with *Punc-104::unc-104::mrfp* (each at a concentration of 75 ng/µl) into *syd-2(ok217)* mutant worms to receive OIW 89 *syd-2(ok217)*;*nthEx89[Punc-104::gfp::syd-2;Punc-104::unc-104::mrfp*]. *Punc-104::mcherry::rab-3* was designed by amplifying the rab-3 gene from cDNA libraries using primers ATGGCGGCTGGCGGACAA (forward) and TTAGCAATTGCATTGCTGTT (reverse). In order to generate transgenic lines expressing cargo markers, we injected existing constructs *Punc-86::snb-1::mRFP* (Wagner et al., 2009) and *Punc-104::mcherry::rab-3* into N2 wild type animals, *unc-10(md1117)* and *syd-2(ok217)* mutants (at a concentration of 100 ng/µl) to obtain strains OIW 90 N2;*nthEx90[Punc-86::snb-1::mRFP],* OIW 91 N2;*nthEx91[Punc-104::mcherry::rab-3],* OIW 92 *syd-2(ok217);nthEx92[Punc-86::snb-1::mRFP],* OIW 93 *syd-2(ok217);nthEx93[Punc-104::mcherry::rab-3],* OIW 94 *unc-10(md1117);nthEx94[Punc-*

86::snb-1::mRFP] and OIW 95 *unc-10(md1117);nthEx95[Punc-104::mcherry::rab-3].* For UNC-104 and RAB-3 colocalization studies, existing plasmids *Punc-104::unc-104ΔPH::gfp* and *Punc-104::mcherry::rab-3 were coinjected into* N2 wild type animals, *unc-10(md1117)* and *syd-2(ok217)* mutants to generate OIW 96 N2;*nthEx96[Punc-104::unc-104ΔPH::gfp;Punc-104::mcherry::rab-3],* OIW 97 *unc-10(md1117)*;*nthEx97[Punc-104::unc-104ΔPH::gfp;Punc-104::mcherry::rab-3]* and OIW 98 *syd-2(ok217);nthEx98[Punc-104::unc-104ΔPH::gfp;Punc-104::mcherry::rab-3]*, respectively. For BiFC experiments *Punc-104::rab-3::VN173* and *Punc-104::snb-1::VC155* plasmids were generated by amplifying *rab-3* cDNA using primers GGCGCGCCATGAATAATCAACAGGC (forward) with an AscI site and ACCGGTGCAATTGCATTGCTGTTGAG (reverse) with an AgeI site and substituted the *map-1* insert in *Punc-104::map-1::VN173* (Wu et al., 2016) with *rab-3*. Similarly, *snb-1* genomic DNA was amplified using primers GGCGCGCCATGGACGCTCAAGGAGATGC (forward) with AscI site and GGTACCTTTTCCTCCAGCCCATAAAACGATGA (reverse) with KpnI site and substituted *lin-2* in *Punc-104::lin-2::VC155* (Wu et al., 2016) with *snb-1*. These plasmids were then co-injected (80 ng/µl) into N2 worms to generate OIW 99 N2;*nthEx99[Punc-104::rab-3::VN173; Punc-104::snb-1::VC155]*. Lastly, *unc-10(md1117);rab-3(js49)* double mutant was generated by crossing *unc-10 (md1117);nthEx[Punc-104*::*unc-104::mrfp]* expressing male worms with *rab-3(js49)* hermaphrodites. Red fluorescent males from the F1 generation exhibiting coiler phenotype were back-crossed into *rab-3(js49)* F_0 hermaphrodites to obtain *unc-10(md1117);rab-3(js49)* homozygous animals.

Real-time PCR

To evaluate *syd-2* RNA levels in *unc-10* and *rab-3* mutants (Figure 1A+B), we performed Real-Time PCR assays employing ABI StepOnePlus Real-Time PCR System in conjunction with the

ABI Power SYBR green PCR master mix. RNA levels of *syd-2* were normalized to *cdc-42* internal control. The following primers were used: CGGAACAATACTCGACTTC (forward) and GCCACACGCTCCATT (reverse) that includes a part of 2nd and 4th exon (200 bp) for *syd-2* and CTGCTGGACAGGAAGATTACG (forward) and TCGGACATTCTCGAATGAAG (reverse) for *cdc-42.*

RNAi feeding assay

RNA interference experiments, we employed the RNAi feeding method (Kamath et al., 2001) in which worms are fed by bacteria expressing individual dsRNA. We obtained feeding clones UNC-10(X-3F06) and SYD-2(X-5K09) from the Julie Ahringer's *C. elegans* RNAi feeding library (Source BioScience LifeSciences, USA; a kind gift of the *C. elegans* Core Facility, Taiwan) which were sequenced to determine their correctness. NGM plates containing ampicillin (25 µg/ml) and 1 mM IPTG were inoculated with the HT115 *E. coli* strain carrying the appropriate dsRNA clone and grown overnight. Fifteen to twenty worms were transferred to the respective RNAi feeding plate and incubated at 20˚C. Worms were then transferred to new RNAi feeding plates every 24 hours and the F1 progeny was used for analysis after day 5. As control, worms were fed with HT115 bacteria containing L4440 empty vector.

Western blotting and Co-Immunoprecipitation Assays

To extract proteins from worms, we prepared lysates from young adults (72 h) based on a previously described protocol (Ward et al., 1988). To perform Western blots from whole worm lysates, 100 µg sample protein was used and membrane blocking was carried out using milk powder for 1-1.5 hours at room temperature (RT). Primary goat N-terminal anti-SYD-2 antibody (cL-19 #sc-15655, Santa Cruz) was incubated at 4°C for 14 hours at 1/500 dilution. Secondary anti-goat antibody was incubated at RT for 2 hours with 1/1000 dilutions. Anti β-actin antibody

was used as control (sc-47778, Santa Cruz). Similarly, 1 mg protein extract was used for immunoprecipitation and incubated with protein G beads and 4 µg mouse anti-GFP antibody (B-2 #sc-9996, Santa Cruz). Western blotting (Figure 1E-H) was performed using a 1:500 dilution of the anti-SYD-2 antibody (primary antibodies dilutions based on the manufacturer's suggestion). Band density analysis was done using NIH ImageJ 1.50 software based on a method published by Schneider et al. (2012).

Worm imaging and motility analysis

For microscopic observations, worms were immobilized on 2% agarose-coated cover slides, and no anesthetics (e.g., levamisole) were used (reported to affect motor motility (Kumar et al., 2010)). A Zeiss LSM780 confocal laser scanning microscope was employed for imaging worms as shown in Figures 2 and 6. For motility analysis (Figure 4) and further imaging (Figure 3 and 5), we employed an Olympus IX81 microscope with a DSU Nipkow spinning disk unit connected to an Andor iXon DV897 EMCCD camera for high-resolution and high-speed time-lapse imaging at 4-5 frames per second. To convert recorded time-lapse sequences into kymographs, we used imaging analysis software NIH ImageJ. The "straighten plugin" was employed to straighten curved axons, and after drawing a line over the axon, the plugin "reslice stack function" was executed to generate kymographs. In kymographs, static particles appear as vertical lines, whereas the slope of a moving particle corresponds to the velocity (speed) of the particle. A pause is defined if motors move less than 0.07 µm/s, and each calculated velocity event does not contain any pauses. On average, we analyzed approximately 600 moving events per experiment from 15 to 25 individual worms. A moving event is defined as a single motility occurrence typically right after a pause or a reversal, and an event ends when the motor again pauses or reverses. Motor cluster analysis (Figures 3B+E) was carried out using ImageJ's "area" tool and the "particle analyze" plugin. To measure travel

distances (Figures 3D and 5F+H) of particles in (straightened) neurons, we used ImageJ's "line tool" to draw a line from the proximal axon hillock to identified distal particle. Intensity Correlation Quotient (ICQ) (Figures 2B, 6D+F) was measured by selecting the region of interest using the "polygonal selection tool" in ImageJ. After background fluorescent intensity subtraction (ImageJ→Process→Subtract Background), the plugin "Intensity Correlation Analysis" was used to generate ICQ values. ICQ values range from -0.5 to 0.5, and values close to 0.5 stand for interdependent expression of two fluorophores, values close to -0.5 stand for segregated expression, and values around 0 imply random expression. For fluorescence intensity quantification (Figure 2D) the following formula was used: Integrated density of selected region – (area of selected region * mean fluorescence of the background) (Li et al., 2004). Parameters such as mean grey value of background, area of selected region and integrated density of selected region was measured using ImageJ. Line scans (Suppl. Figure S3 and S4) were generated using ImageJ (ImageJ→Analyze→Plot profile) after straightening the neurite using the ImageJ plugin "straighten". Further these values from ImageJ are plotted using MS Excel.

ACKNOWLEDGEMENTS

We thank the *C. elegans* Core Facility (CECF) Taiwan (funded by the Ministry of Science and Technology, MOST) for providing microinjection setups and worm observation systems. We acknowledge MOST grant NSC 100-2311-B-007-004 to OIW and support by the Brain Research Center of National Tsing Hua University under the Higher Education Sprout Project funded by the Ministry of Science and Technology and Ministry of Education in Taiwan.

REFERENCES

Ackermann, F., C.L. Waites, and C.C. Garner. 2015. Presynaptic active zones in invertebrates and vertebrates. *EMBO Rep*. 16:923-938.

Barnes, A.P., and F. Polleux. 2009. Establishment of axon-dendrite polarity in developing neurons. *Annu Rev Neurosci*. 32:347-381.

Brady, S.T., and G.A. Morfini. 2017. Regulation of motor proteins, axonal transport deficits and adult-onset neurodegenerative diseases. *Neurobiol Dis*. 105:273-282.

Brenner, S. 1974. The genetics of Caenorhabditis elegans. *Genetics*. 77:71-94.

Breuss, M., and D.A. Keays. 2014. Microtubules and neurodevelopmental disease: the movers and the makers. *Adv Exp Med Biol*. 800:75-96.

Brooks, B.R. 1991. The role of axonal transport in neurodegenerative disease spread: a meta-analysis of experimental and clinical poliomyelitis compares with amyotrophic lateral sclerosis. *Can J Neurol Sci*. 18:435-438.

Campbell, R.E., O. Tour, A.E. Palmer, P.A. Steinbach, G.S. Baird, D.A. Zacharias, and R.Y. Tsien. 2002. A monomeric red fluorescent protein. *Proc Natl Acad Sci U S A*. 99:7877-7882.

Chia, P.H., M.R. Patel, O.I. Wagner, D.R. Klopfenstein, and K. Shen. 2013. Intramolecular regulation of presynaptic scaffold protein SYD-2/liprin-alpha. *Mol Cell Neurosci*. 56:76-84.

Dai, Y., H. Taru, S.L. Deken, B. Grill, B. Ackley, M.L. Nonet, and Y. Jin. 2006. SYD-2 Liprin-alpha organizes presynaptic active zone formation through ELKS. *Nat Neurosci*. 9:1479-1487.

Edwards, S.L., R.M. Yorks, L.M. Morrison, C.M. Hoover, and K.G. Miller. 2015. Synapse-Assembly Proteins Maintain Synaptic Vesicle Cluster Stability and Regulate Synaptic Vesicle Transport in Caenorhabditis elegans. *Genetics*. 201:91-116.

Fischer von Mollard, G., B. Stahl, C. Li, T.C. Sudhof, and R. Jahn. 1994. Rab proteins in regulated exocytosis. *Trends Biochem Sci*. 19:164-168.

Franker, M.A., and C.C. Hoogenraad. 2013. Microtubule-based transport - basic mechanisms, traffic rules and role in neurological pathogenesis. *J Cell Sci*. 126:2319-2329.

Geppert, M., V.Y. Bolshakov, S.A. Siegelbaum, K. Takei, P. De Camilli, R.E. Hammer, and T.C. Sudhof. 1994. The role of Rab3A in neurotransmitter release. *Nature*. 369:493-497.

Goodwin, P.R., and P. Juo. 2013. The scaffolding protein SYD-2/Liprin-alpha regulates the mobility and polarized distribution of dense-core vesicles in C. elegans motor neurons. *PloS one*. 8:e54763.

Gracheva, E.O., G. Hadwiger, M.L. Nonet, and J.E. Richmond. 2008. Direct interactions between C. elegans RAB-3 and Rim provide a mechanism to target vesicles to the presynaptic density. *Neurosci Lett*. 444:137-142.

Hall, D.H., and E.M. Hedgecock. 1991. Kinesin-related gene unc-104 is required for axonal transport of synaptic vesicles in C. elegans. *Cell*. 65:837-847.

Hsu, C.C., J.D. Moncaleano, and O.I. Wagner. 2011. SUB-CELLULAR DISTRIBUTION OF UNC-104(KIF1A) UPON BINDING TO ADAPTORS AS UNC-16(JIP3), DNC-1(DCTN1/Glued) AND SYD-2(LIPRIN-alpha) IN C. ELEGANS NEURONS. *Neuroscience*. 176:39-52.

Hu, C.D., and T.K. Kerppola. 2003. Simultaneous visualization of multiple protein interactions in living cells using multicolor fluorescence complementation analysis. *Nat Biotechnol*. 21:539-545.
Johnston, P.A., B.T. Archer, 3rd, K. Robinson, G.A. Mignery, R. Jahn, and T.C. Sudhof. 1991. rab3A attachment to the synaptic vesicle membrane mediated by a conserved polyisoprenylated carboxy-terminal sequence. *Neuron*. 7:101-109.
Kamath, R.S., M. Martinez-Campos, P. Zipperlen, A.G. Fraser, and J. Ahringer. 2001. Effectiveness of specific RNA-mediated interference through ingested double-stranded RNA in Caenorhabditis elegans. *Genome Biol*. 2:RESEARCH0002.
Kapitein, L.C., and C.C. Hoogenraad. 2011. Which way to go? Cytoskeletal organization and polarized transport in neurons. *Mol Cell Neurosci*. 46:9-20.
Kittelmann, M., J. Hegermann, A. Goncharov, H. Taru, M.H. Ellisman, J.E. Richmond, Y. Jin, and S. Eimer. 2013. Liprin-alpha/SYD-2 determines the size of dense projections in presynaptic active zones in C. elegans. *J Cell Biol*. 203:849-863.
Klopfenstein, D.R., M. Tomishige, N. Stuurman, and R.D. Vale. 2002. Role of phosphatidylinositol(4,5)bisphosphate organization in membrane transport by the Unc104 kinesin motor. *Cell*. 109:347-358.
Klopfenstein, D.R., and R.D. Vale. 2004. The lipid binding pleckstrin homology domain in UNC-104 kinesin is necessary for synaptic vesicle transport in Caenorhabditis elegans. *Mol Biol Cell*. 15:3729-3739.
Ko, J., S. Kim, J.G. Valtschanoff, H. Shin, J.R. Lee, M. Sheng, R.T. Premont, R.J. Weinberg, and E. Kim. 2003. Interaction between liprin-alpha and GIT1 is required for AMPA receptor targeting. *J Neurosci*. 23:1667-1677.
Koushika, S.P., J.E. Richmond, G. Hadwiger, R.M. Weimer, E.M. Jorgensen, and M.L. Nonet. 2001. A post-docking role for active zone protein Rim. *Nat Neurosci*. 4:997-1005.
Kumar, J., B.C. Choudhary, R. Metpally, Q. Zheng, M.L. Nonet, S. Ramanathan, D.R. Klopfenstein, and S.P. Koushika. 2010. The Caenorhabditis elegans Kinesin-3 motor UNC-104/KIF1A is degraded upon loss of specific binding to cargo. *PLoS Genet*. 6:e1001200.
Lemmon, M.A., and K.M. Ferguson. 2001. Molecular determinants in pleckstrin homology domains that allow specific recognition of phosphoinositides. *Biochem Soc Trans*. 29:377-384.
Li, J.Y., R. Jahn, and A. Dahlstrom. 1995. Rab3a, a small GTP-binding protein, undergoes fast anterograde transport but not retrograde transport in neurons. *Eur J Cell Biol*. 67:297-307.
Li, Q., A. Lau, T.J. Morris, L. Guo, C.B. Fordyce, and E.F. Stanley. 2004. A syntaxin 1, Galpha(o), and N-type calcium channel complex at a presynaptic nerve terminal: analysis by quantitative immunocolocalization. *J Neurosci*. 24:4070-4081.
Luo, L. 2002. Actin cytoskeleton regulation in neuronal morphogenesis and structural plasticity. *Annu Rev Cell Dev Biol*. 18:601-635.
Maday, S., A.E. Twelvetrees, A.J. Moughamian, and E.L. Holzbaur. 2014. Axonal transport: cargo-specific mechanisms of motility and regulation. *Neuron*. 84:292-309.
Maeder, C.I., A. San-Miguel, E.Y. Wu, H. Lu, and K. Shen. 2014. In vivo neuron-wide analysis of synaptic vesicle precursor trafficking. *Traffic*. 15:273-291.

Mahoney, T.R., Q. Liu, T. Itoh, S. Luo, G. Hadwiger, R. Vincent, Z.W. Wang, M. Fukuda, and M.L. Nonet. 2006. Regulation of synaptic transmission by RAB-3 and RAB-27 in Caenorhabditis elegans. *Mol Biol Cell*. 17:2617-2625.

Millecamps, S., and J.P. Julien. 2013. Axonal transport deficits and neurodegenerative diseases. *Nat Rev Neurosci*. 14:161-176.

Niwa, S., D.M. Lipton, M. Morikawa, C. Zhao, N. Hirokawa, H. Lu, and K. Shen. 2016. Autoinhibition of a Neuronal Kinesin UNC-104/KIF1A Regulates the Size and Density of Synapses. *Cell Rep*. 16:2129-2141.

Niwa, S., Y. Tanaka, and N. Hirokawa. 2008. KIF1Bbeta- and KIF1A-mediated axonal transport of presynaptic regulator Rab3 occurs in a GTP-dependent manner through DENN/MADD. *Nat Cell Biol*. 10:1269-1279.

Nonet, M.L., K. Grundahl, B.J. Meyer, and J.B. Rand. 1993. Synaptic function is impaired but not eliminated in C. elegans mutants lacking synaptotagmin. *Cell*. 73:1291-1305.

Nonet, M.L., O. Saifee, H. Zhao, J.B. Rand, and L. Wei. 1998. Synaptic transmission deficits in Caenorhabditis elegans synaptobrevin mutants. *J Neurosci*. 18:70-80.

Nonet, M.L., J.E. Staunton, M.P. Kilgard, T. Fergestad, E. Hartwieg, H.R. Horvitz, E.M. Jorgensen, and B.J. Meyer. 1997. Caenorhabditis elegans rab-3 mutant synapses exhibit impaired function and are partially depleted of vesicles. *J Neurosci*. 17:8061-8073.

Perlson, E., S. Maday, M.M. Fu, A.J. Moughamian, and E.L. Holzbaur. 2010. Retrograde axonal transport: pathways to cell death? *Trends Neurosci*. 33:335-344.

Rashid, D.J., J. Bononi, B.P. Tripet, R.S. Hodges, and D.W. Pierce. 2005. Monomeric and dimeric states exhibited by the kinesin-related motor protein KIF1A. *J Pept Res*. 65:538-549.

Richens, J.L., J.S. Lane, J.P. Bramble, and P. O'Shea. 2015. The electrical interplay between proteins and lipids in membranes. *Biochim Biophys Acta*. 1848:1828-1836.

Schneider, C.A., W.S. Rasband, and K.W. Eliceiri. 2012. NIH Image to ImageJ: 25 years of image analysis. *Nature methods*. 9:671-675.

Schoch, S., P.E. Castillo, T. Jo, K. Mukherjee, M. Geppert, Y. Wang, F. Schmitz, R.C. Malenka, and T.C. Sudhof. 2002. RIM1alpha forms a protein scaffold for regulating neurotransmitter release at the active zone. *Nature*. 415:321-326.

Shin, H., M. Wyszynski, K.H. Huh, J.G. Valtschanoff, J.R. Lee, J. Ko, M. Streuli, R.J. Weinberg, M. Sheng, and E. Kim. 2003. Association of the kinesin motor KIF1A with the multimodular protein liprin-alpha. *J Biol Chem*. 278:11393-11401.

Spangler, S.A., and C.C. Hoogenraad. 2007. Liprin-alpha proteins: scaffold molecules for synapse maturation. *Biochem Soc Trans*. 35:1278-1282.

Spangler, S.A., S.K. Schmitz, J.T. Kevenaar, E. de Graaff, H. de Wit, J. Demmers, R.F. Toonen, and C.C. Hoogenraad. 2013. Liprin-alpha2 promotes the presynaptic recruitment and turnover of RIM1/CASK to facilitate synaptic transmission. *J Cell Biol*. 201:915-928.

Stigloher, C., H. Zhan, M. Zhen, J. Richmond, and J.L. Bessereau. 2011. The presynaptic dense projection of the Caenorhabditis elegans cholinergic neuromuscular junction localizes synaptic vesicles at the active zone through SYD-2/liprin and UNC-10/RIM-dependent interactions. *J Neurosci*. 31:4388-4396.

Taru, H., and Y. Jin. 2011. The Liprin homology domain is essential for the homomeric interaction of SYD-2/Liprin-alpha protein in presynaptic assembly. *J Neurosci*. 31:16261-16268.

Tien, N.W., G.H. Wu, C.C. Hsu, C.Y. Chang, and O.I. Wagner. 2011. Tau/PTL-1 associates with kinesin-3 KIF1A/UNC-104 and affects the motor's motility characteristics in C. elegans neurons. *Neurobiol Dis*. 43:495-506.

Tomishige, M., D.R. Klopfenstein, and R.D. Vale. 2002. Conversion of Unc104/KIF1A kinesin into a processive motor after dimerization. *Science*. 297:2263-2267.

Vershinin, M., B.C. Carter, D.S. Razafsky, S.J. King, and S.P. Gross. 2007. Multiple-motor based transport and its regulation by Tau. *Proc Natl Acad Sci U S A*. 104:87-92.

Wagner, O.I., A. Esposito, B. Kohler, C.W. Chen, C.P. Shen, G.H. Wu, E. Butkevich, S. Mandalapu, D. Wenzel, F.S. Wouters, and D.R. Klopfenstein. 2009. Synaptic scaffolding protein SYD-2 clusters and activates kinesin-3 UNC-104 in C. elegans. *Proc Natl Acad Sci U S A*. 106:19605-19610.

Wang, Y., M. Okamoto, F. Schmitz, K. Hofmann, and T.C. Sudhof. 1997. Rim is a putative Rab3 effector in regulating synaptic-vesicle fusion. *Nature*. 388:593-598.

Wang, Y., S. Sugita, and T.C. Sudhof. 2000. The RIM/NIM family of neuronal C2 domain proteins. Interactions with Rab3 and a new class of Src homology 3 domain proteins. *J Biol Chem*. 275:20033-20044.

Ward, S., D.J. Burke, J.E. Sulston, A.R. Coulson, D.G. Albertson, D. Ammons, M. Klass, and E. Hogan. 1988. Genomic organization of major sperm protein genes and pseudogenes in the nematode Caenorhabditis elegans. *J Mol Biol*. 199:1-13.

Wu, G.H., M. Muthaiyan Shanmugam, P. Bhan, Y.H. Huang, and O.I. Wagner. 2016. Identification and Characterization of LIN-2(CASK) as a Regulator of Kinesin-3 UNC-104(KIF1A) Motility and Clustering in Neurons. *Traffic*. 17:891-907.

Wu, Y.E., L. Huo, C.I. Maeder, W. Feng, and K. Shen. 2013. The balance between capture and dissociation of presynaptic proteins controls the spatial distribution of synapses. *Neuron*. 78:994-1011.

Xuan, Z., L. Manning, J. Nelson, J.E. Richmond, D.A. Colon-Ramos, K. Shen, and P.T. Kurshan. 2017. Clarinet (CLA-1), a novel active zone protein required for synaptic vesicle clustering and release. *Elife*. 6.

Yonekawa, Y., A. Harada, Y. Okada, T. Funakoshi, Y. Kanai, Y. Takei, S. Terada, T. Noda, and N. Hirokawa. 1998. Defect in synaptic vesicle precursor transport and neuronal cell death in KIF1A motor protein-deficient mice. *J Cell Biol*. 141:431-441.

Zhang, Y.V., S.B. Hannan, Z.A. Stapper, J.V. Kern, T.R. Jahn, and T.M. Rasse. 2016. The Drosophila KIF1A Homolog unc-104 Is Important for Site-Specific Synapse Maturation. *Front Cell Neurosci*. 10:207.

Zhen, M., and Y. Jin. 1999. The liprin protein SYD-2 regulates the differentiation of presynaptic termini in C. elegans. *Nature*. 401:371-375.

Zhen, M., and Y. Jin. 2004. Presynaptic terminal differentiation: transport and assembly. *Curr Opin Neurobiol*. 14:280-287.

FIGURE LEGENDS

Figure 1: Real-Time PCR and co-immunoprecipitation analysis to investigate genetic and functional relations between syd-2, unc-10 and rab-3 in *C. elegans*. (A+B) Relative syd-2 RNA (extracted from worm lysates) expression levels in two different *unc-10* allelic backgrounds (A) and in a *rab-3* mutant (B). RNA levels were normalized to *cdc-42* (internal control). (C) SYD-2 protein expression changes in two different *unc-10* allelic backgrounds (A) and in a *rab-3* mutant (B). Data revealed from Western blot band intensity measurements and representative Western blot example shown in (E, "Lysate") and (G, "Lysate"). (E) Immunoprecipitation of UNC-104 and detection of bound SYD-2 (using anti-SYD-2 antibody) in lysates from worms expressing UNC-104::GFP either in wild type or in *unc-10* allelic backgrounds. (F) Quantification of data from (E). SYD-2 band signal intensities in each sample is normalized against IgG. For antibody details, refer to the Methods and Materials section). P-values: *P<0.05, **P<0.01, ***P<0.001, ****P<0.0001 (Student's t-test). Box plots represent min to max values. No of trials for each experimental group = 3.

Figure 2: Colocalization and BiFC between UNC-104 and SYD-2 in the presence and absence of *unc-10* and *rab-3*. (A) UNC-104 and SYD-2 colocalization in the nerve ring of wild type, *unc-10*, *rab-3*, and *unc-10;rab-3* worms. White arrows highlight specific colocalization events. (B) Intensity correlation coefficients from images shown in (A) (n = 20 worms). (C) UNC-104 and SYD-2 BiFC signals in the nerve ring of wild type, *unc-10* and *rab-3* worms. UNC-104/UNC-104 used as positive and UNC-104/empty (empty vector) used as negative BiFC control. White dashed lines indicate the borders of the worm's head. (D) Fluorescence intensity measurements from images shown in (C) (n = 25 worms). A = anterior, P = posterior directions (in (C)). P-values:

*P<0.05, **P<0.01, ***P<0.001, ****P<0.0001 (Student's t-test). Box plots represent min to max values. Scale bar: 10 µm.

Figure 3: Effect of *syd-2*, *unc-10* and *rab-3* (single and double mutants) on UNC-104 clustering in sublateral nerve bundles and single ALM neurons. (A) UNC-104 cluster patterning in sublateral nerve bundles. (B) Cluster size (area) quantification from (A). (C) Stacks of ALM neurons (after digital straightening) reflect characteristic UNC-104 cluster patterning in different mutants. (D) Quantification of average distances travelled from the axonal hillock (red dotted line in (C)) to distal areas in the neuron (data taken from (C)). (E) Cluster size (area) quantification from (C). P-values: *P<0.05, **P<0.01, ***P<0.001, ****P<0.0001 (Student's t-test). Box plots represent min to max values. N = 20 worms per experimental group. Scale bar: 10 µm.

Figure 4: Effect of *syd-2*, *unc-10* and *rab-3* (single and double mutants) on UNC-104 motility. (A) Anterograde velocity of UNC-104 in *syd-2, unc-10, rab-3* single mutants as well as in various double mutant combinations. Green dotted lines outline critical data set comparisons. (B) UNC-104 anterograde run length. Red wild cards indicates t-tests between *unc-10* and *unc-10;rab-3* double mutants. (C) Anterograde moving persistency of UNC-104. (D) UNC-104 pausing behavior. Red wild cards indicate t-tests between between *unc-10* and *unc-10;rab-3* double mutants. Analyzed total events: UNC-104(wt) = 689, *syd-2(ok217)* = 535, *unc-10(md1117)* = 515, *rab-3(js49)* = 520, *unc-10;rab-3* double mutant= 522, *syd-2(ok217);unc-10* RNAi = 536, r*ab-3(js49);syd-2* RNAi = 518, *rab-3* rescue = 535, *syd-2* rescue = 323, *unc-10* rescue = 495, *syd-2* overexpression = 595, *syd-2* overexpression*;unc-10* RNAi = 570. P-values: *P<0.05, **P<0.01, ***P<0.001, ****P<0.0001 (Student's t-test). Box plots represent min to max values.

Figure 5: Effect of *syd-2*, *unc-10* and *rab-3* (single and double mutants) on SNB-1 and RAB-3 cargo trafficking. (A) Anterograde velocities of SNB-1-tagged synaptic vesicles. (B) Anterograde velocities of RAB-3-tagged synaptic vesicles. (C) Anterograde run lengths of SNB-1-tagged synaptic vesicles. (D) Anterograde run lengths of RAB-3-tagged synaptic vesicles. (E) Stacks of ALM neurons unravels characteristic SNB-1 cluster patterning in different mutants. (F) Quantification of average distances travelled from the axonal hillock (red dotted line in (E)) to distal areas in the neuron (data taken from (E); n = 20 worms). (G) Stacks of ALM neurons to demonstrate RAB-3 cluster patterning in different mutants. (H) Quantification of average distances travelled from the axonal hillock (red dotted line in (G)) to distal areas in the neuron (data taken from (G); n = 20 worms). Analyzed total moving events in (A-D): SNB-1(wt) = 510, *rab-3* RNAi = 360, *syd-2(ok217)* = 439, *unc-10(md1117)* = 518, *unc-10(md1117);syd-2* RNAi = 250, RAB-3(wt)= 513, *snb-1* RNAi = 306, *syd-2(ok217)* = 508, *unc-10(md1117)* = 509 and *unc-10(md1117);syd-2* RNAi = 300. P-values: *P<0.05, **P<0.01, ***P<0.001, ****P<0.0001 (Student's t-test). Box plots represent min to max values. Scale bar: 10 µm.

Figure 6: Interaction between RAB-3/UNC-104 and SNB-1/UNC-104 in the presence or absence of the motor's PH domain. (A) RAB-3 colocalization with full length UNC-104. (B) RAB-3 colocalization with UNC-104 lacking the PH domain (UNC-104ΔPH). (C) Colocalization of UNC-104ΔPH and RAB-3 in *syd-2* and *unc-10* knockout worms. (D) Quantification of data from (A-C). (E) SNB-1 colocalization with full length UNC-104 (wt and *unc-10* mutant) as well as with UNC-104 lacking the PH domain. (F) Quantification of data from (E). (G-H) Colocalization of UNC-104ΔPH/SNB-1 and UNC-104ΔPH/RAB-3 in dorsal and ventral nerve cords. P-values: *P<0.05, **P<0.01, ***P<0.001, ****P<0.0001 (Student's t-test). Box plots represent min to max values. N = 20 worms for all experimental groups. Scale bar: 10 µm.

Figure 7: Model of the UNC-10/SYD-2 receptor in UNC-104-mediated RAB-3 cargo transport. (A) Current model of unspecific UNC-104-vesicle interactions. (B) Loss of UNC-10/SYD-2 linker negatively affects RAB-3 cargo transport mediated by UNC-104 in *C. elegans* neurons. (C) Presence of UNC-10/SYD-2 promotes RAB-3 cargo transport.

FIGURES

FIGURE 1

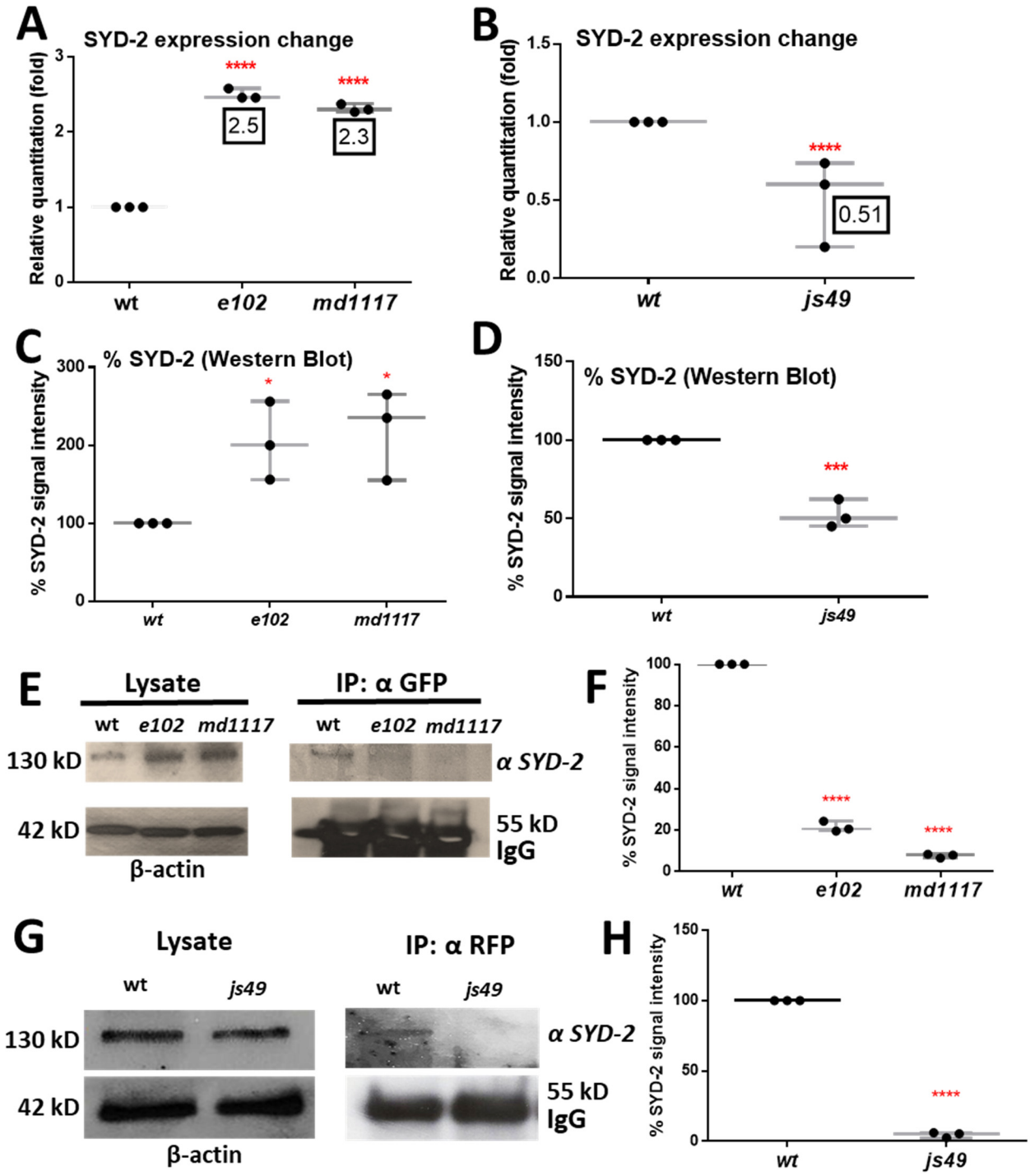

FIGURE 2

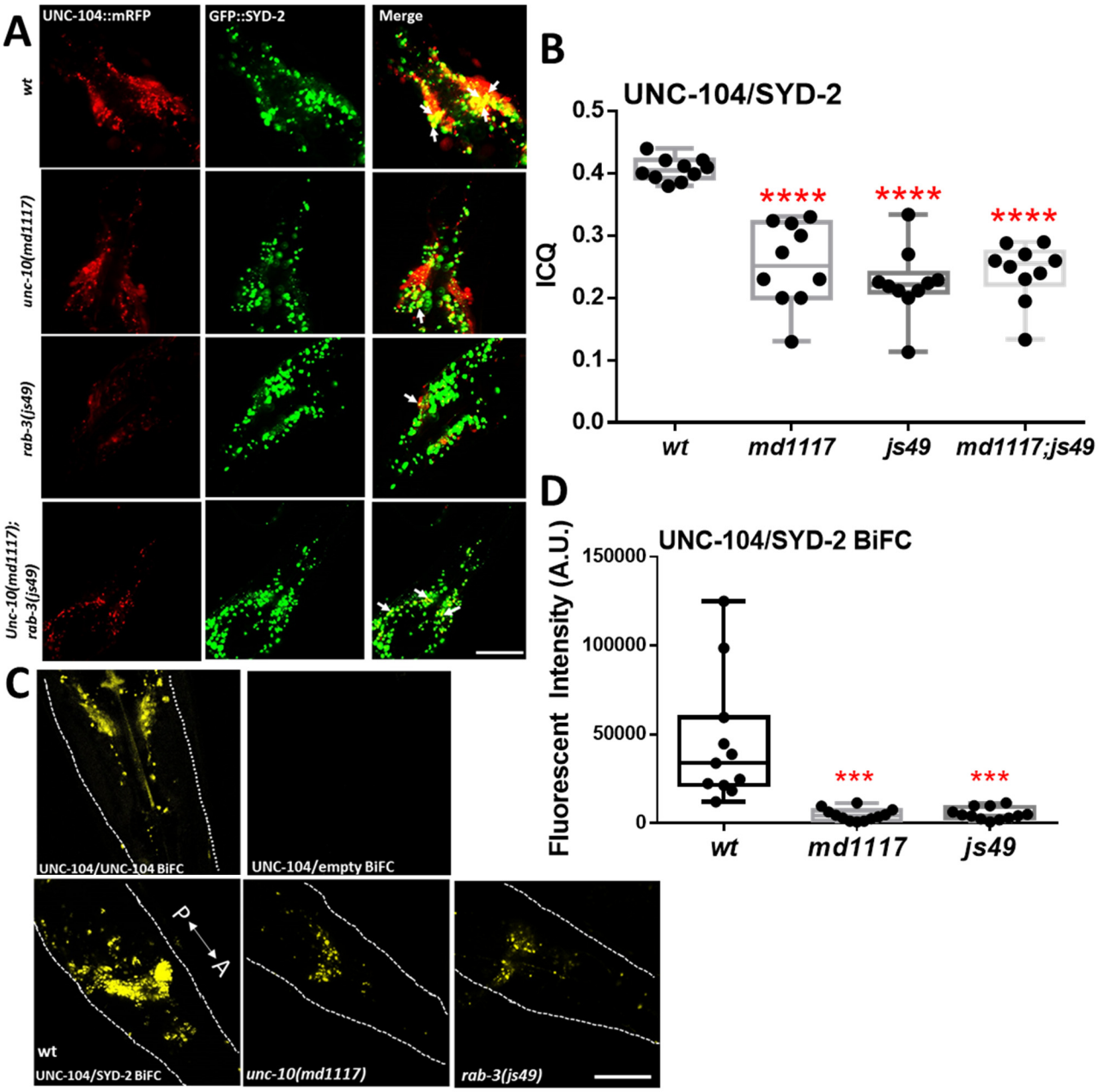
A
UNC-104::mRFP
GFP::SYD-2
Merge
wt
unc-10(md1117)
rab-3(js49)
Unc-10(md1117); rab-3(js49)
B
UNC-104/SYD-2
ICQ
0.5
0.4
0.3
0.2
0.1
0.0
****
****
****
wt
md1117
js49
md1117;js49
C
UNC-104/UNC-104 BiFC
UNC-104/empty BiFC
P
A
wt
UNC-104/SYD-2 BiFC
unc-10(md1117)
rab-3(js49)
D
UNC-104/SYD-2 BiFC
Fluorescent Intensity (A.U.)
150000
100000
50000
0
***
***
wt
md1117
js49

FIGURE 3

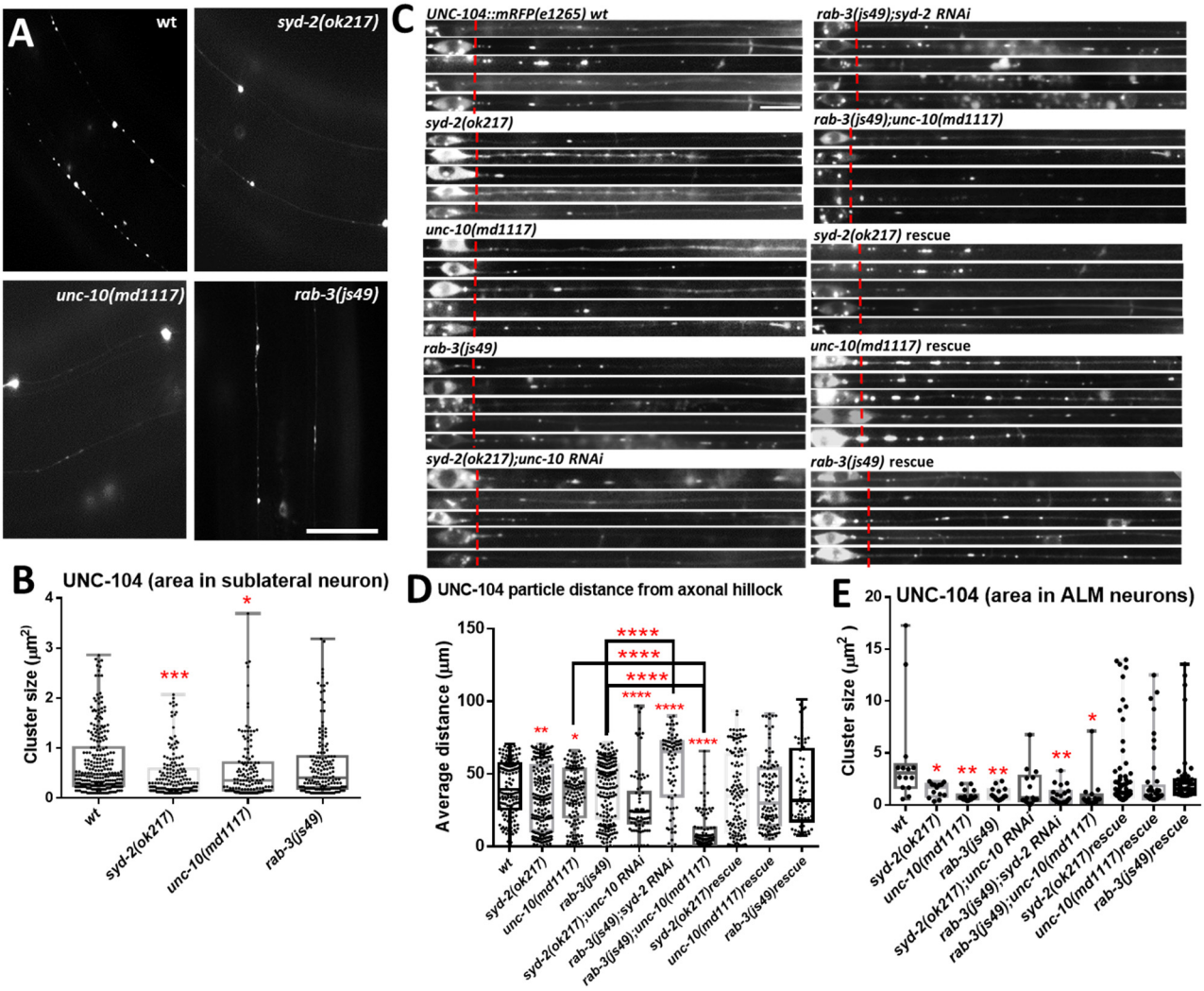
A
wt
syd-2(ok217)
unc-10(md1117)
rab-3(js49)
C
UNC-104::mRFP(e1265) wt
syd-2(ok217)
unc-10(md1117)
rab-3(js49)
syd-2(ok217);unc-10 RNAi
rab-3(js49);syd-2 RNAi
rab-3(js49);unc-10(md1117)
syd-2(ok217) rescue
unc-10(md1117) rescue
rab-3(js49) rescue
B
UNC-104 (area in sublateral neuron)
Cluster size (μm²)
D
UNC-104 particle distance from axonal hillock
Average distance (μm)
E
UNC-104 (area in ALM neurons)
Cluster size (μm²)

FIGURE 4

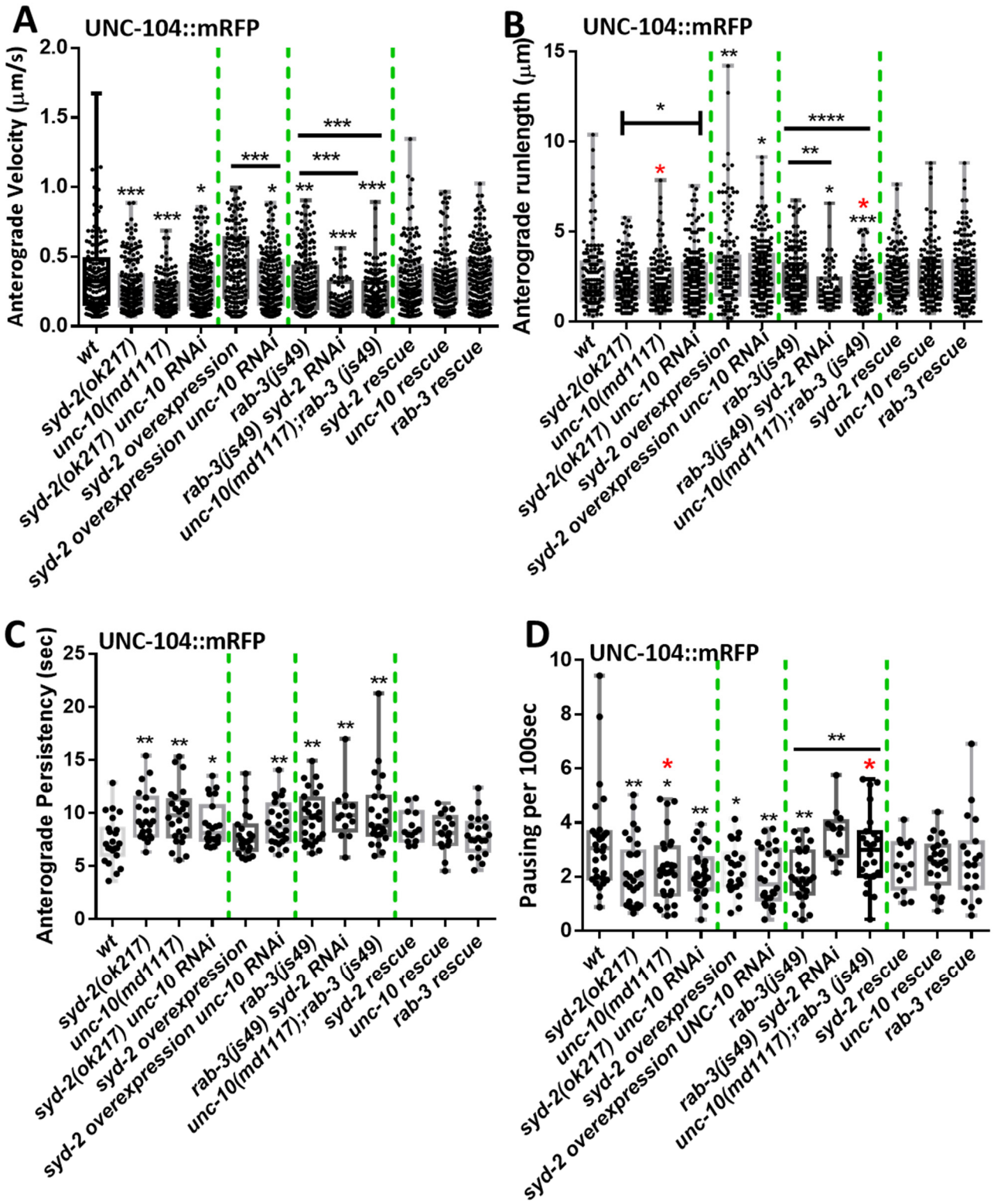
A
UNC-104::mRFP
Anterograde Velocity (μm/s)
B
UNC-104::mRFP
Anterograde runlength (μm)
C
UNC-104::mRFP
Anterograde Persistency (sec)
D
UNC-104::mRFP
Pausing per 100sec
wt
syd-2(ok217)
unc-10(md1117)
syd-2(ok217) unc-10 RNAi
syd-2 overexpression
syd-2 overexpression unc-10 RNAi
rab-3(js49)
rab-3(js49) syd-2 RNAi
unc-10(md1117);rab-3 (js49)
syd-2 rescue
unc-10 rescue
rab-3 rescue

FIGURE 5

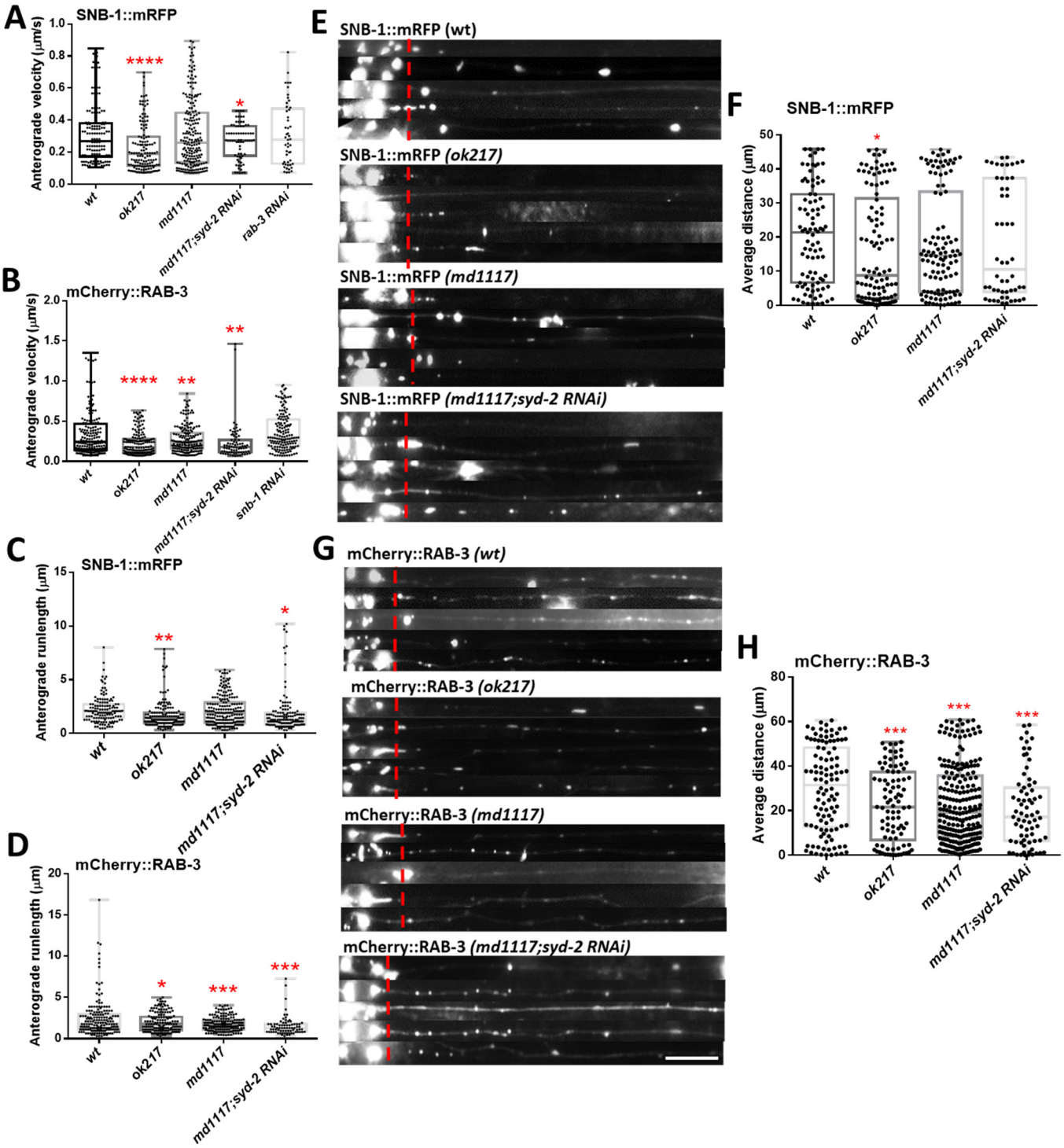
A
SNB-1::mRFP
Anterograde velocity (µm/s)
1.0
0.8
0.6
0.4
0.2
0.0
****
*
wt
ok217
md1117
md1117;syd-2 RNAi
rab-3 RNAi
B
mCherry::RAB-3
Anterograde velocity (µm/s)
2.0
1.5
1.0
0.5
0.0
****
**
**
wt
ok217
md1117
md1117;syd-2 RNAi
snb-1 RNAi
C
SNB-1::mRFP
Anterograde runlength (µm)
15
10
5
0
**
*
wt
ok217
md1117
md1117;syd-2 RNAi
D
mCherry::RAB-3
Anterograde runlength (µm)
20
15
10
5
0
*
***
***
wt
ok217
md1117
md1117;syd-2 RNAi
E
SNB-1::mRFP (wt)
SNB-1::mRFP (ok217)
SNB-1::mRFP (md1117)
SNB-1::mRFP (md1117;syd-2 RNAi)
F
SNB-1::mRFP
Average distance (µm)
50
40
30
20
10
0
*
wt
ok217
md1117
md1117;syd-2 RNAi
G
mCherry::RAB-3 (wt)
mCherry::RAB-3 (ok217)
mCherry::RAB-3 (md1117)
mCherry::RAB-3 (md1117;syd-2 RNAi)
H
mCherry::RAB-3
Average distance (µm)
80
60
40
20
0
***
***
***
wt
ok217
md1117
md1117;syd-2 RNAi

FIGURE 6

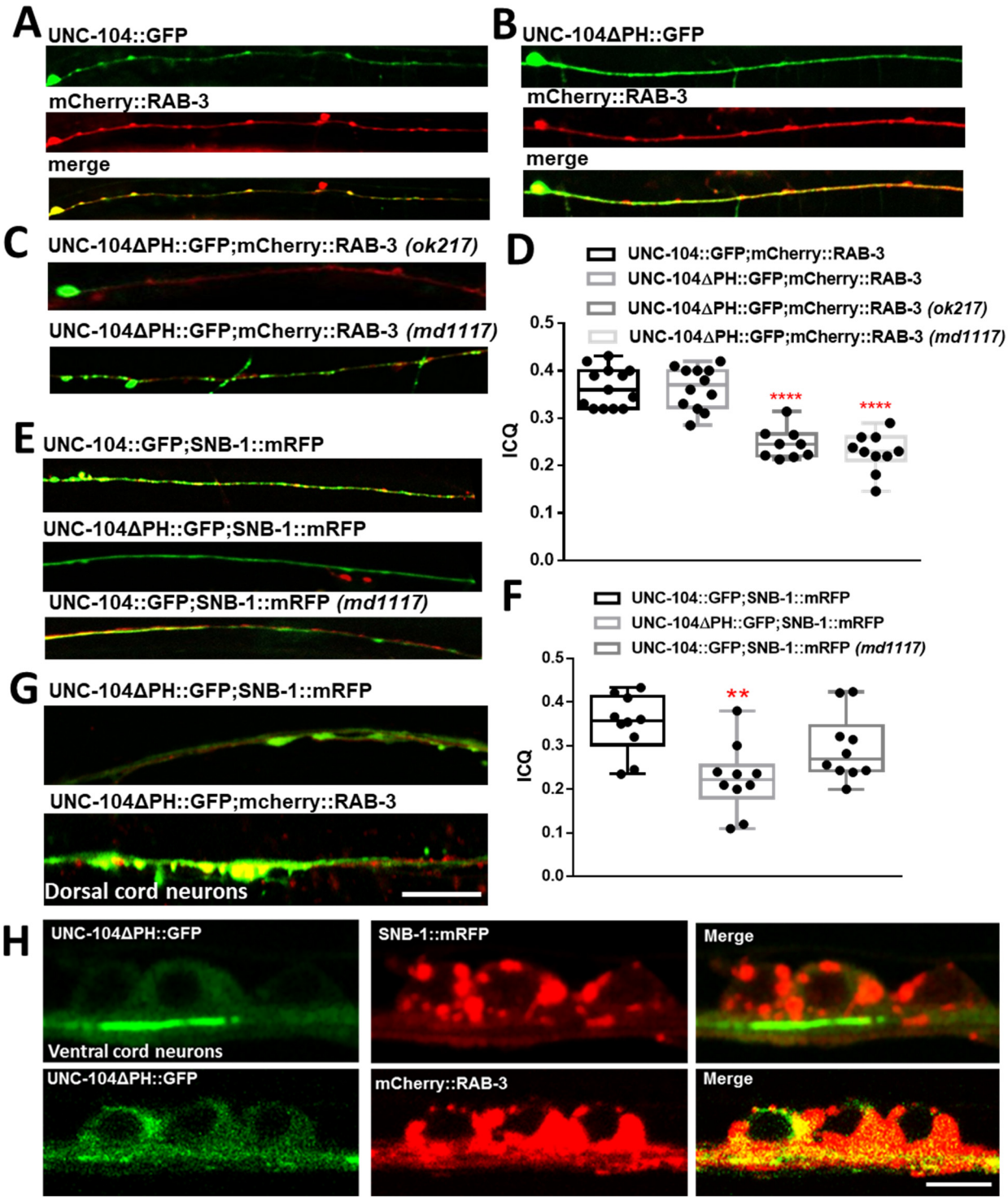
A
UNC-104::GFP
mCherry::RAB-3
merge
B
UNC-104ΔPH::GFP
mCherry::RAB-3
merge
C
UNC-104ΔPH::GFP;mCherry::RAB-3 (ok217)
UNC-104ΔPH::GFP;mCherry::RAB-3 (md1117)
D
UNC-104::GFP;mCherry::RAB-3
UNC-104ΔPH::GFP;mCherry::RAB-3
UNC-104ΔPH::GFP;mCherry::RAB-3 (ok217)
UNC-104ΔPH::GFP;mCherry::RAB-3 (md1117)
ICQ
0.5
0.4
0.3
0.2
0.1
0.0
****
****
E
UNC-104::GFP;SNB-1::mRFP
UNC-104ΔPH::GFP;SNB-1::mRFP
UNC-104::GFP;SNB-1::mRFP (md1117)
F
UNC-104::GFP;SNB-1::mRFP
UNC-104ΔPH::GFP;SNB-1::mRFP
UNC-104::GFP;SNB-1::mRFP (md1117)
ICQ
0.5
0.4
0.3
0.2
0.1
0.0
**
G
UNC-104ΔPH::GFP;SNB-1::mRFP
UNC-104ΔPH::GFP;mcherry::RAB-3
Dorsal cord neurons
H
UNC-104ΔPH::GFP
SNB-1::mRFP
Merge
Ventral cord neurons
UNC-104ΔPH::GFP
mCherry::RAB-3
Merge

FIGURE 7

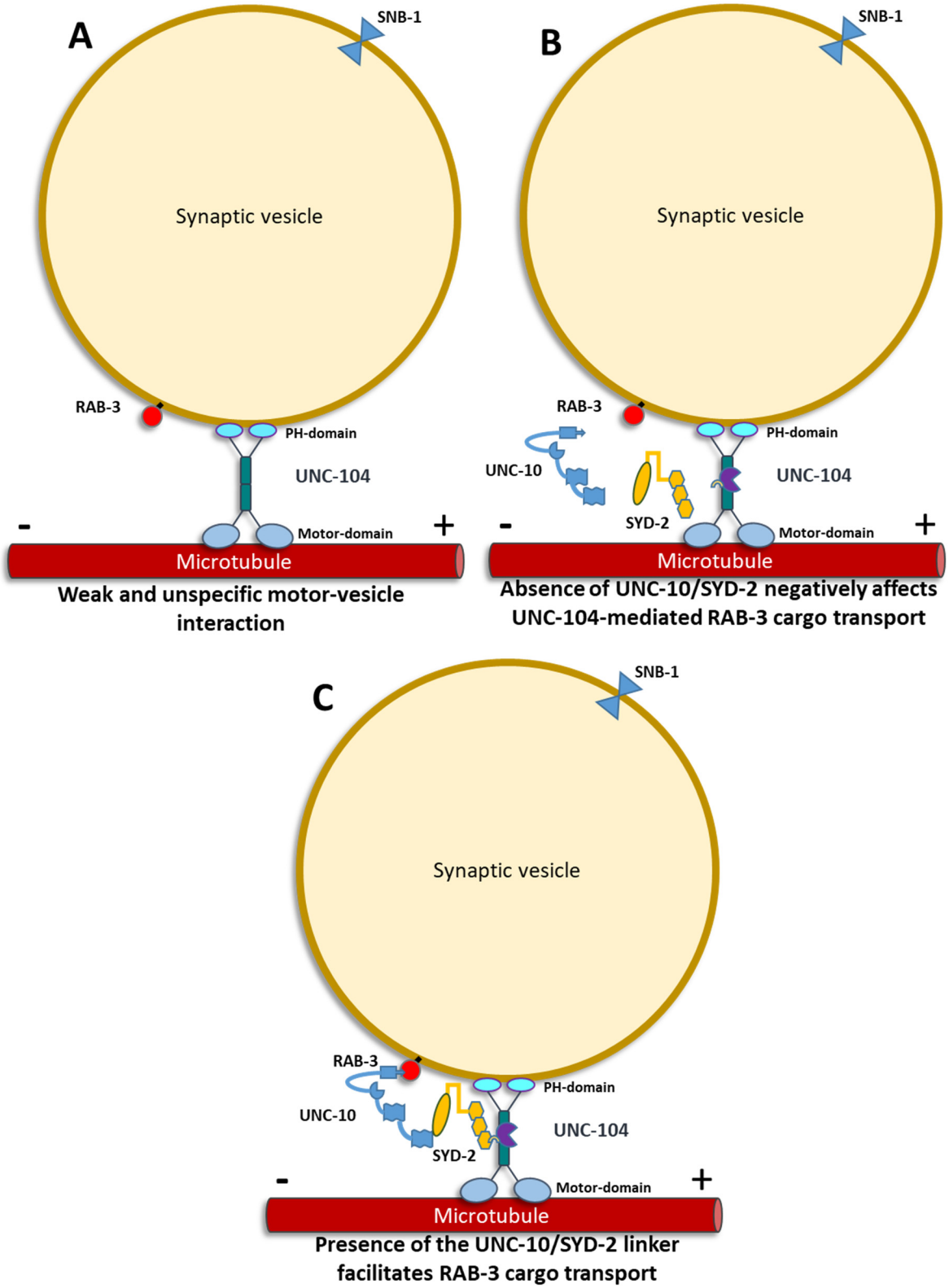
A
SNB-1
Synaptic vesicle
RAB-3
PH-domain
UNC-104
-
+
Motor-domain
Microtubule
Weak and unspecific motor-vesicle interaction
B
SNB-1
Synaptic vesicle
RAB-3
PH-domain
UNC-10
UNC-104
SYD-2
-
+
Motor-domain
Microtubule
Absence of UNC-10/SYD-2 negatively affects UNC-104-mediated RAB-3 cargo transport
C
SNB-1
Synaptic vesicle
RAB-3
PH-domain
UNC-10
UNC-104
SYD-2
-
+
Motor-domain
Microtubule
Presence of the UNC-10/SYD-2 linker facilitates RAB-3 cargo transport

SUPPLEMENTARY MATERIAL

SUPPLEMENTARY FIGURE LEGENDS

Suppl. Figure S1: (A) Schematic domain structures of UNC-104, UNC-10, SYD-2 and RAB-3. Available mutant alleles (carrying the respective gene alone) are marked in red. (B) Cartoon explaining the determination of a particle's average travel distance in axons. (C) Kymograph representing various motility parameters.

Suppl. Figure S2: (A) Frequency distribution of UNC-104 anterograde velocities (from Figure 4A). (B) Frequency distribution of UNC-104 anterograde run lengths (from Figure 4B).

Suppl. Figure S3: (A-D) Line scans along neurons in images as displayed in Figure 6A-C.

Suppl. Figure S4: (A-D) Line scans along neurons in images as displayed in Figure 6E.

SUPPLEMENTARY FIGURES

SUPPLEMENTARY FIGURE S1

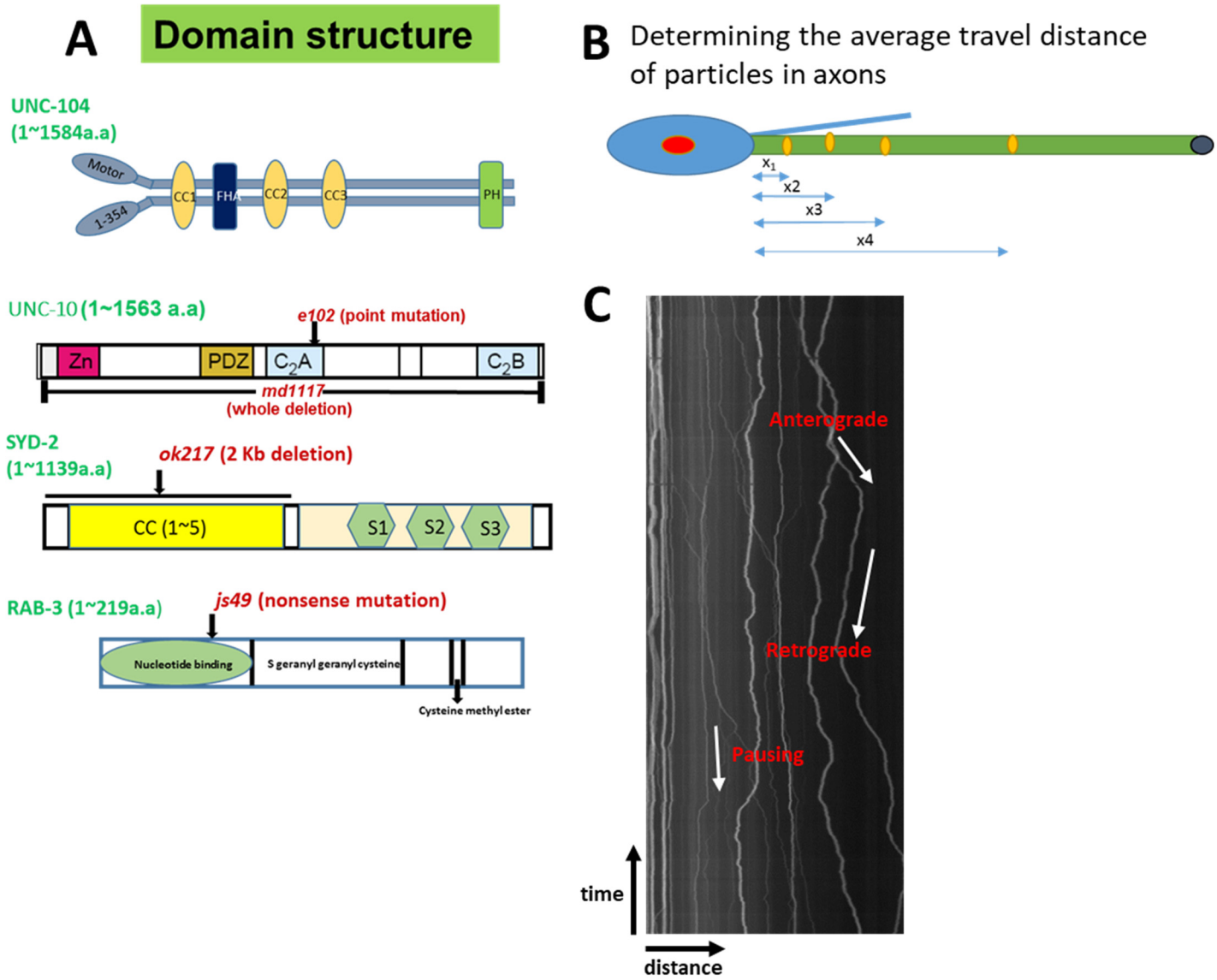

SUPPLEMENTARY FIGURE S2

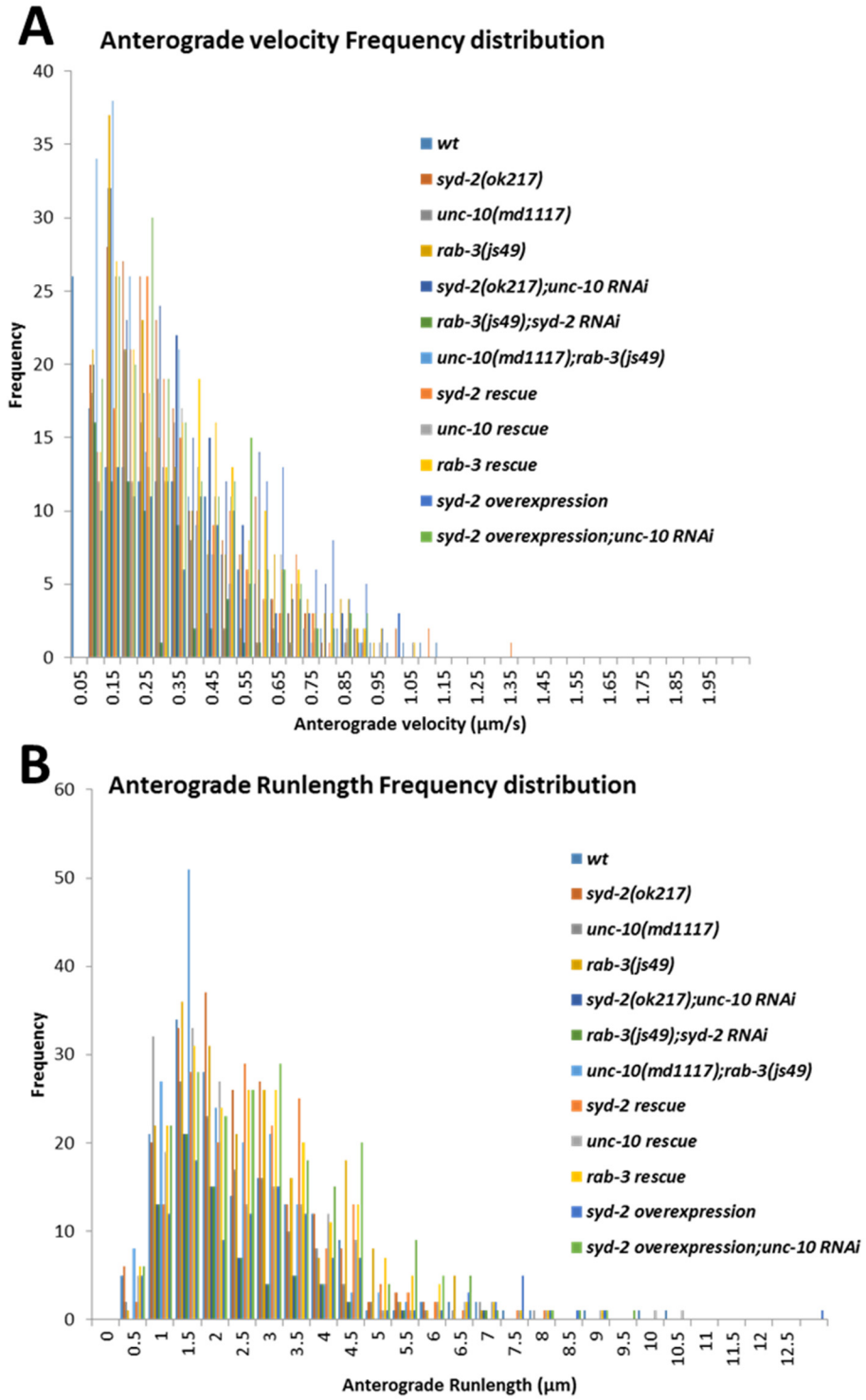

SUPPLEMENTARY FIGURE S3

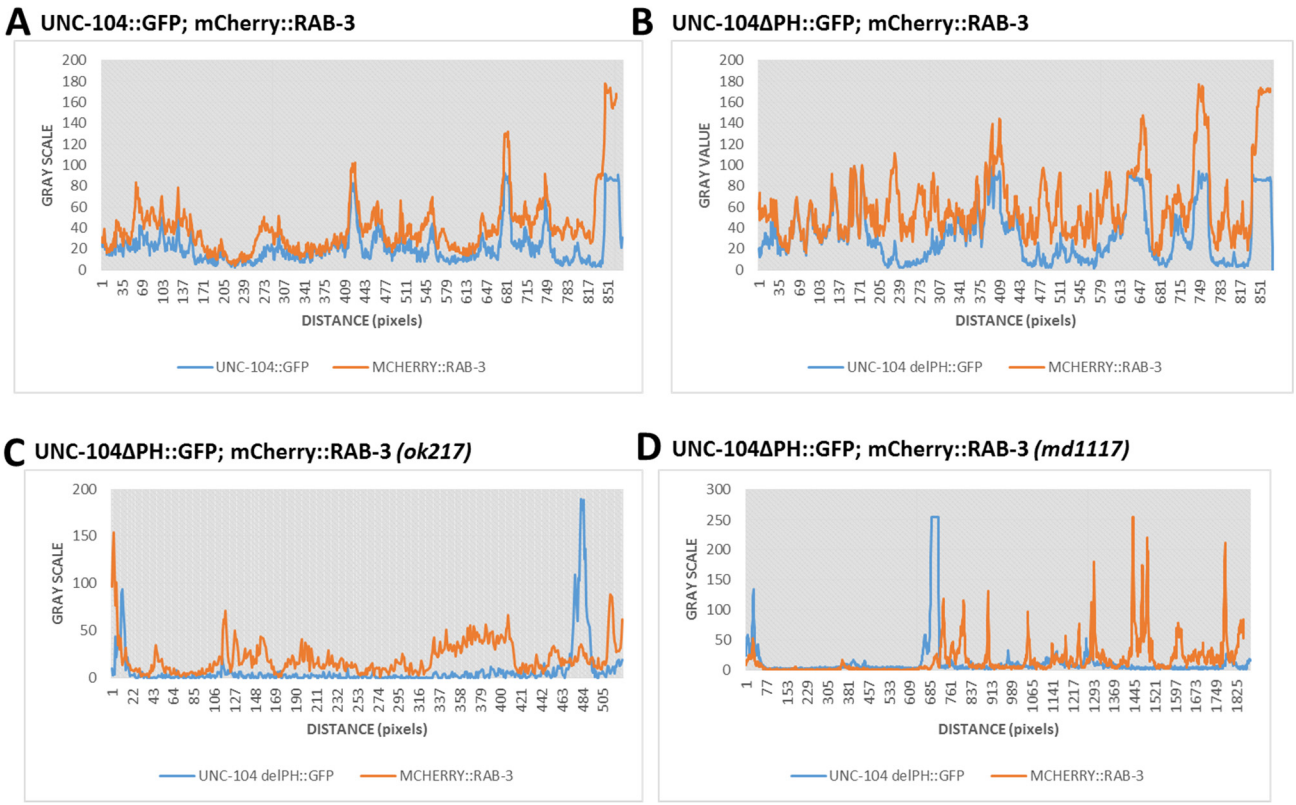

SUPPLEMENTARY FIGURE S4

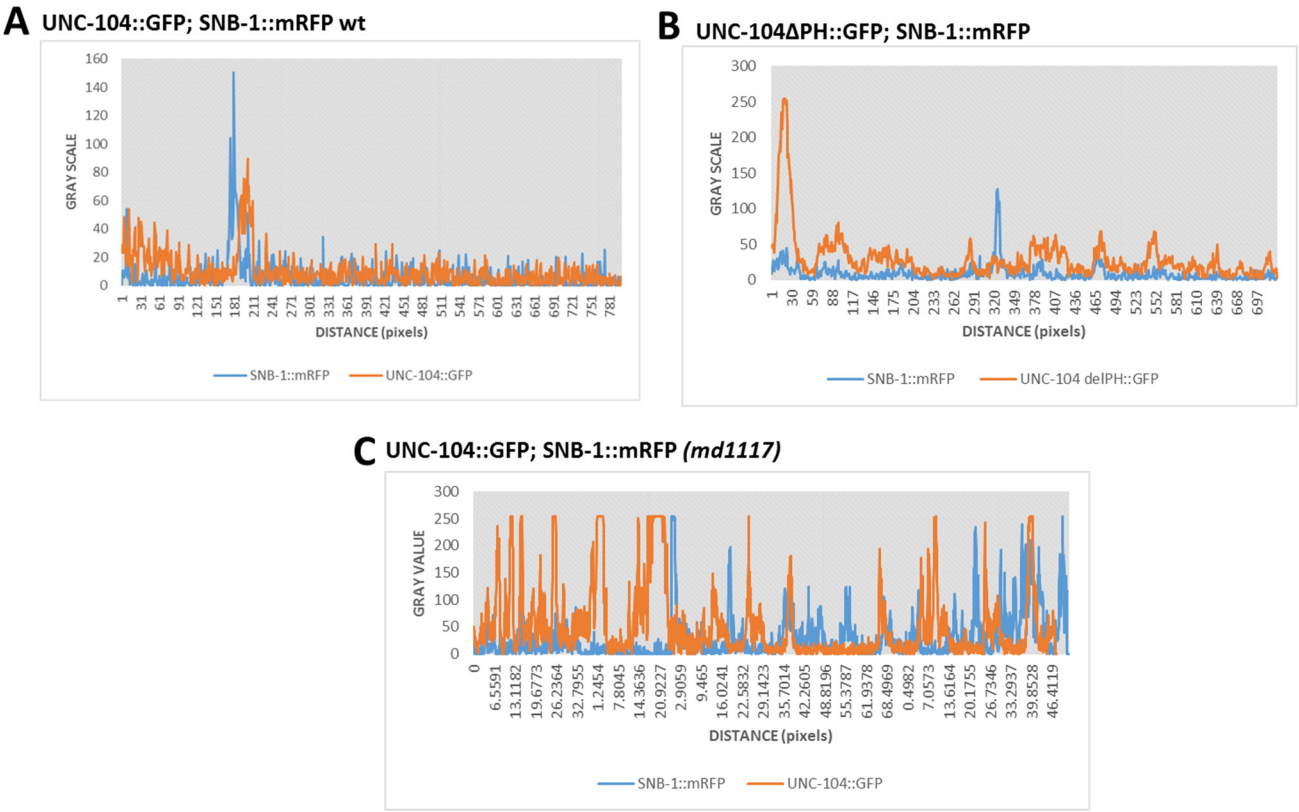

SUPPLEMENTARY TABLE LEGENDS

Supplementary Table S1: Accompanying table with details to Figure 3B.

Supplementary Table S2: Accompanying table with details to Figure 3D+E.

Supplementary Table S3: Accompanying table with details to Figure 4A+B.

Supplementary Table S4: Accompanying table with details to Figure 4C+D.

Supplementary Table S5: Accompanying table with details to Figure 5A-D.

Supplementary Table S6: Accompanying table with details to Figure 5F+H.

SUPPLEMENTARY TABLES

Suppl. Table S1

UNC-104 ::mRFP	wt	*syd-2 (ok217)*	*unc-10 (md1117)*	*rab-3 (js49)*
Average cluster size(μM^2)	**0.72±0.64**	**0.474±0.38**	**0.574±0.48**	**0.655±0.56**
Total neurite length (mm)	1.95	2.44	1.44	1.28
Cluster per 100µm	19.55	15.5	22.7	25.4
# cluster	382	380	330	326

Suppl. Table S2

	Average distance (µm)	Cluster size (μm^2)
UNC-104::mRFP	Mean±SEM	Mean±SEM
wt	40.77±1.510	4.458±1.253
syd-2(ok217)	34.26±1.563	1.445±0.189
unc-10(md1117)	35.60±1.602	0.883±0.119
rab-3(js49)	39.63±1.432	1.021±0.413
syd-2(ok217)unc-10 RNAi	29.30±2.442	1.702±0.502
rab-3(js49)syd-2 RNAi	54.41±2.866	0.898±0.177
rab-3(js49);unc-10(md1117)	9.809±1.255	0.976±0.420
syd-2 rescue	35.99±2.472	2.522±0.383
unc-10 rescue	36.07±2.346	2.304±0.486
rab-3 rescue	40.01±3.316	2.599±0.458

Suppl. Table S3

	Anterograde Velocity (µm/s)			Anterograde runlength (µm)	
UNC-104::mRFP	Mean	SEM	N	Mean	SEM
wt	0.378	0.021	165	2.430	0.137
syd-2(ok217)	0.280	0.012	193	2.203	0.082
unc-10(md1117)	0.230	0.010	155	2.139	0.113
rab-3(js49)	0.306	0.015	194	2.483	0.098
syd-2(ok217)unc-10 RNAi	0.321	0.012	223	2.487	0.098
rab-3(js49)syd-2 RNAi	0.214	0.015	170	1.936	0.130
rab-3(js49);unc-10(md1117)	0.224	0.011	172	1.863	0.076
Syd-2 overexpression	0.438	0.020	155	3.021	0.183
Syd-2 overexpression; unc-10 RNAi	0.321	0.013	207	2.792	0.114
syd-2 rescue	0.331	0.016	175	2.563	0.099
unc-10 rescue	0.327	0.016	161	2.679	0.128
rab-3 rescue	0.353	0.015	202	2.590	0.110

Suppl. Table S4

	Anterograde persistency (sec)		Pausing per 100 sec	
UNC-104::mRFP	Mean	SEM	Mean	SEM
wt	7.425	0.459	3.257	0.333
syd-2(ok217)	9.727	0.484	2.179	0.220
unc-10(md1117)	9.830	0.521	2.264	0.220
rab-3(js49)	9.607	0.448	2.067	0.175
syd-2(ok217)unc-10 RNAi	8.925	0.430	2.150	0.165
rab-3(js49)syd-2 RNAi	9.982	0.727	3.570	0.263
rab-3(js49);unc-10(md1117)	9.982	0.693	3.008	0.279
Syd-2 overexpression	7.969	0.425	2.288	0.190
Syd-2 overexpression; unc-10 RNAi	9.112	0.401	1.978	0.199
syd-2 rescue	8.642	0.402	2.449	0.231
unc-10 rescue	8.230	0.405	2.486	0.190
rab-3 rescue	7.886	0.412	2.658	0..339

Suppl. Table S5

	Anterograde Velocity (µm/s)			Anterograde runlength (µm)	
SNB-1::mRFP	Mean	SEM	N	Mean	SEM
wt	0.317	0.015	158	2.243	0.106
syd-2(ok217)	0.230	0.012	159	1.798	0.115
unc-10(md1117)	0.315	0.014	203	2.411	0.123
unc-10(md1117);syd-2 RNAi	0.270	0.012	72	1.837	0.160
Rab-3 RNAi	0.3104	0.028	149		
mCherry::RAB-3					
wt	0.351	0.021	174	2.451	0.170
syd-2(ok217)	0.226	0.011	158	1.970	0.092
unc-10(md1117)	0.275	0.012	182	1.768	0.064
unc-10(md1117);syd-2 RNAi	0.233	0.026	74	1.527	0.132
Snb-1 RNAi	0.367	0.018	184		

Suppl. Table S6

	SNB-1::mRFP	mCherry::RAB-3
	Average distance (µm)	Average distance (µm)
wt	20.49±1.503	29.93±1.839
syd-2(ok217)	16.13±1.507	22.41±1.706
unc-10(md1117)	18.03±1.431	22.81±1.142
unc-10(md1117);syd-2 RNAi	18.16±2.290	20.38±1.986